

Local PCA Shows How the Effect of Population Structure Differs Along the Genome

Han Li¹, Peter Ralph^{1,2,3,*}

1 Department of Molecular and Computational Biology, University of Southern California, Los Angeles, CA , USA

2 Institute of Ecology and Evolution, University of Oregon, Eugene, OR, USA

3 Department of Mathematics, University of Oregon, Eugene, OR, USA

*** plr@uoregon.edu**

Abstract

Population structure leads to systematic patterns in measures of mean relatedness between individuals in large genomic datasets, which are often discovered and visualized using dimension reduction techniques such as principal component analysis (PCA). Mean relatedness is an average of the relationships across locus-specific genealogical trees, which can be strongly affected on intermediate genomic scales by linked selection and other factors. We show how to use local principal components analysis to describe this meso-scale heterogeneity in patterns of relatedness, and apply the method to genomic data from three species, finding in each that the effect of population structure can vary substantially across only a few megabases. In a global human dataset, localized heterogeneity is likely explained by polymorphic chromosomal inversions. In a range-wide dataset of *Medicago truncatula*, factors that produce heterogeneity are shared between chromosomes, correlate with local gene density, and may be caused by background selection or local adaptation. In a dataset of primarily African *Drosophila melanogaster*, large-scale heterogeneity across each chromosome arm is explained by known chromosomal inversions thought to be under recent selection, and after removing samples carrying inversions, remaining heterogeneity is correlated with recombination rate and gene density, again suggesting a role for linked selection. The visualization method provides a flexible new way to discover biological drivers of genetic variation, and its application to data highlights the strong effects that linked selection and chromosomal inversions can have on observed patterns of genetic variation.

1 Introduction

To-do: cite Duforet-Frebourg et al. (2015).

Wright (1949) defined *population structure* to encompass “such matters as numbers, composition by age and sex, and state of subdivision”, where “subdivision” refers to restricted migration between subpopulations. The phrase is also commonly used to refer to the genetic patterns that result from this process, as for instance reduced mean relatedness between individuals from distinct populations. However, it is not necessarily clear what aspects of demography should be included in the concept. For instance, Blair (1943) defines *population structure* to be the sum total of “such factors as size of breeding populations, periodic fluctuation of population size, sex ratio, activity range and *differential survival of progeny*” (emphasis added). The definition is similar to Wright’s, but differs in including the effects of natural selection. On closer examination, incorporating differential survival or fecundity makes the concept less clear: should a randomly mating population consisting of two types that are partially reproductively isolated from each other be said to show population structure or not? Whatever the definition, it is clear that due to natural selection, the effects of population structure – the *realized* patterns of genetic relatedness – differ depending on which portion of the genome is being considered. For instance, strongly locally adapted alleles of a gene will be selected against in migrants to different habitats, increasing genetic differentiation between populations near to this gene. Similarly, newly adaptive alleles spread first in local populations. These observations motivate many methods to search for genetic loci under selection, as for example in Huerta-Sánchez et al. (2013) and Martin et al. (2016).

These realized patterns of genetic relatedness summarize the shapes of the genealogical trees at each location along the genome. Since these trees vary along the genome, so does relatedness, but averaging over sufficiently many trees we hope to get a stable estimate that doesn’t depend much on the genetic markers chosen. This is not guaranteed: for instance, relatedness on sex chromosomes is expected to differ from the autosomes; and positive or negative selection on particular loci can dramatically distort shapes of nearby genealogies (Barton 2000; Charlesworth et al. 1993; Kim and Stephan 2002). Indeed, many species show chromosome-scale variation in diversity and divergence (e.g., (Langley et al. 2012)); species phylogenies can differ along the genome due to incomplete lineage sorting, adaptive introgression and/or local adaptation (e.g., (Ellegren et al. 2012; Nadeau et al. 2012; Pease and Hahn 2013; Pool 2015; Vernot and Akey 2014)); and theoretical expectations predict that geographic patterns of relatedness should depend on selection (Charlesworth et al. 2003).

Patterns in genome-wide relatedness are often summarized by applying principal components analysis (PCA, (Patterson et al. 2006)) to the genetic covariance matrix, as pioneered by Menozzi et al. (1978). The results of PCA can be related to the genealogical history of the samples, such as time to most recent common ancestor and migration rate between populations (McVean 2009; Novembre and Stephens 2008), and sometimes produce “maps” of population structure that reflect the samples’ geographic origin distorted by rates of gene flow (Novembre et al. 2008).

Modeling such “background” kinship between samples is essential to genome-wide asso-

ciation studies (GWAS, (Astle and Balding 2009; Price et al. 2006)), and so understanding variation in kinship along the genome could lead to more generally powerful methods, and may be essential for doing GWAS in species with substantial heterogeneity in realized patterns of mean relatedness along the genome.

A note on nomenclature: In this work we describe variation in patterns of relatedness using local PCA, where “local” refers to proximity along the genome. A number of general methods for dimensionality reduction also use a strategy of “local PCA” (e.g., (Kambhatla and Leen 1997; Manjón et al. 2013; Roweis and Saul 2000; Weingessel and Hornik 2000)), performing PCA not on the entire dataset but instead on subsets of observations, providing local pictures which are then stitched back together to give a global picture. At first sight, this differs from our method in that we restrict to subsets of *variables* instead of subsets of observations. However, if we flip perspectives and think of each genetic variant as an observation, our method shares common threads, although our method does not subsequently use adjacency along the genome, as we aim to identify similar regions that may be distant.

As reviewed above, it is common to describe variation along the genome of simple statistics such as F_{ST} , and also to use methods such as PCA to visualize large-scale patterns in genome-wide relatedness. In this paper we apply PCA locally along the genome, thus describing in an unbiased, descriptive way how patterns of mean relatedness vary systematically along the genome, in a way particularly suited to large samples from geographically distributed populations. Geographic population structure sets the stage by establishing similar patterns of relatedness across much of the genome; we then aim to describe how this structure is affected by selection and other factors. Our aim is not to identify outlier loci, but rather to describe larger-scale variation shared by many parts of the genome. By doing this with three taxa with diverse population histories, we can compare relative contributions of different sorts of variation across taxa; since the method is an visualization method, we allow ourselves to be surprised by unexpected signals in the data.

2 Materials and Methods

As depicted in Figure 1, the general steps to the method are: (1) divide the genome into windows, (2) summarize the patterns of relatedness in each window, (3) measure dissimilarity in relatedness between each pair of windows, (4) visualize the resulting dissimilarity matrix using multidimensional scaling (MDS), and (5) combine similar windows to more accurately visualize local effects of population structure using PCA.

2.1 PCA in genomic windows

To begin, we first recoded sampled genotypes as numeric matrices in the usual manner, by recording the number of nonreference alleles seen at each locus for each sample. We then

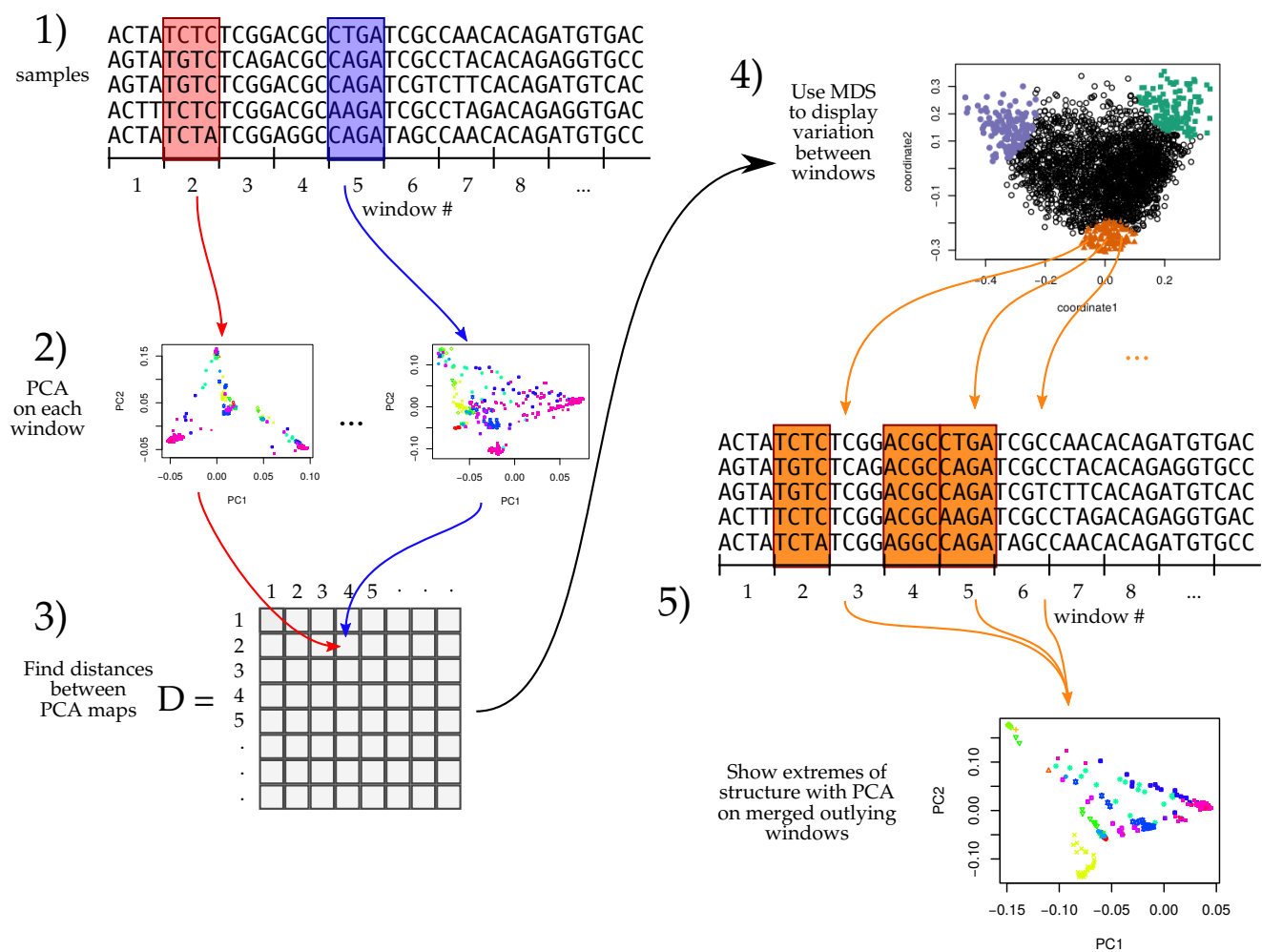


Figure 1: An illustration of the method; see Methods for details.

divided the genome into contiguous segments (“windows”) and applied principal component analysis (PCA) as described in McVean (2009) separately to the submatrices that corresponded to each window. The choice of window length entails a tradeoff between signal and noise, since shorter windows allow better resolution along the genome but provide less precise estimates of relatedness. A method for choosing a window length to balance these considerations is given in Appendix A. Precisely, denote by Z the $L \times N$ recoded genotype matrix for a given window (L is the number of SNPs and N is the sample size), and by \overline{Z}_s the mean of non-missing entries for allele s , so that $\overline{Z}_s = \frac{1}{n_s} \sum_j Z_{sj}$, where the sum is over the n_s nonmissing genotypes. We first compute the mean-centered matrix X , as $X_{si} = Z_{si} - \overline{Z}_s$, and preserving missingness. (This mean-centering makes the result not depend on the choice of reference allele, exactly if there is no missing data, and approximately otherwise.) Next, we find the covariance matrix of X , denoted C , as $C_{ij} = \frac{1}{m_{ij}-1} \sum_s X_{si} X_{sj} - \frac{1}{m_{ij}(m_{ij}-1)} (\sum_s X_{si}) (\sum_s X_{sj})$, where all sums are over the m_{ij} sites where both sample i and sample j have nonmissing genotypes. The principal components are the eigenvectors of C , normalized to have Euclidean length equal to one, and ordered by magnitude of the eigenvalues.

The top few principal components are generally good summaries of population structure; we follow common practice and usually only use the first two (referred to as $PC1$ and $PC2$). The above procedure can be performed on any subset of the data; for future reference, denote by $PC1_j$ and $PC2_j$ the result after applying to all SNPs in the j^{th} window.

Since the definition of eigenvectors does not specify their sign, when comparing between windows we choose signs to best match each other: after choosing $PC1_1$, for instance, if u is the first eigenvector obtained from the covariance matrix for window j , then we next choose $PC1_j = \pm u$, where the sign is chosen according to which of $\|PC1_1 - u\|$ or $\|PC1_1 + u\|$ is smaller.

Several of the datasets we use have unbalanced representations of diverged populations, which can have a strong impact on the results of PCA. (The principal axes may describe variation *within* an overrepresented group rather than more significant variation between groups.) Therefore, to check that sampling patterns do not affect our results, we compared to a variant of PCA that gives roughly equal weight to each group of samples, rather than to each sample. The rationale and implementation of this method are described in Appendix B.

2.2 Similarity of patterns of relatedness between windows

We think of the local effects of population structure as being summarized by *relative* position of the samples in the space defined by the top principal components. However, we do not compare patterns of relatedness of different genomic regions by directly comparing the PCs, since rotations or reflections of these imply identical patterns of relatedness. Instead, we compare the low-dimensional approximations of the local covariance matrices

149 obtained using the top k PCs, which is invariant under reflections and rotations and yet
 150 contains all other information about the PCs. (For results shown here, we use $k = 2$; results
 151 using larger numbers of PCs were nearly identical.) Furthermore, to remove the effect of
 152 artifacts such as mutation rate variation, we also rescale each approximate covariance
 153 matrix to be of similar size (precisely, so that the underlying data matrix has trace norm
 154 equal to one).

155 To do this, define the $N \times k$ matrix $V(i)$ so that $V(i)_{\cdot\ell}$, the ℓ^{th} column of $V(i)$, is
 156 equal to the ℓ^{th} principal component of the i^{th} window, multiplied by $(\lambda_{\ell i} / \sum_{m=1}^k \lambda_{mi})^{1/2}$,
 157 where $\lambda_{\ell i}$ is the ℓ^{th} eigenvalue of the genetic covariance matrix. Then, the rescaled, rank
 158 k approximate covariance matrix for the i^{th} window is

$$M(i) = \sum_{\ell=1}^k V(i)_{\cdot\ell} V(i)_{\cdot\ell}^T. \quad (1)$$

159 To measure the similarity of patterns of relatedness for the i^{th} window and j^{th} win-
 160 dow, we then use Euclidean distance D_{ij} between the matrices $M(i)$ and $M(j)$: $D_{ij}^2 =$
 161 $\sum_{k,\ell} (M(i)_{k,\ell} - M(j)_{k,\ell})^2$.

162 The goal of comparing PC plots up to rotation and reflection turned out to be equivalent
 163 to comparing rank- k approximations to local covariance matrices. This suggests instead
 164 directly comparing entire local covariance matrices. However, with thousands of samples
 165 and tens of thousands of windows, computing the distance matrix would take months
 166 of CPU time, while as defined above, D can be computed in minutes using the following
 167 method. Since for square matrices A and B , $\sum_{ij} (A_{ij} - B_{ij})^2 = \sum_{ij} (A_{ij}^2 + B_{ij}^2) - 2 \text{tr}(A^T B)$,
 168 then due to the orthogonality of eigenvectors and the cyclic invariance of trace, D_{ij} can be
 169 computed efficiently as

$$D_{ij} = \left(\frac{\sum_{\ell=1}^k \lambda_{\ell i}^2}{(\sum_{\ell=1}^k \lambda_{\ell i})^2} + \frac{\sum_{\ell=1}^k \lambda_{\ell j}^2}{(\sum_{\ell=1}^k \lambda_{\ell j})^2} - 2 \sum_{\ell,m=1}^k (V(i)^T V(j))_{\ell m}^2 \right)^{1/2}. \quad (2)$$

170 2.3 Visualization of results

171 We use multidimensional scaling (MDS) to visualize relationships between windows as
 172 summarized by the dissimilarity matrix D . MDS produces a set of m coordinates for
 173 each window that give the arrangement in m -dimensional space that best recapitulates the
 174 original distance matrix. For results here, we use $m = 2$ to produce one- or two-dimensional
 175 visualizations of relationships between windows' patterns of relatedness.

176 We then locate variation in patterns of relatedness along the genome by choosing col-
 177 lections of windows that are nearby in MDS coordinates, and map their positions along the
 178 genome. A visualization of the effects of population structure across the entire collection
 179 is formed by extracting the corresponding genomic regions and performing PCA on all,
 180 aggregated, regions.

181 2.4 Datasets

182 We applied the method to genomic datasets with good geographic sampling: 380 African
183 *Drosophila melanogaster* from the Drosophila Genome Nexus (Lack et al. 2015), a world-
184 wide dataset of humans, 3,965 humans from several locations worldwide from the POPRES
185 dataset (Nelson et al. 2008), and 263 *Medicago truncatula* from 24 countries around the
186 Mediterranean basin a range-wide dataset of the partially selfing weedy annual plant from
187 the *Medicago truncatula* Hapmap Project (Tang et al. 2014), as summarized in Table 1.

188 ***Drosophila melanogaster:*** We used whole-genome sequencing data from the Drosophila
189 Genome Nexus (<http://www.johnpool.net/genomes.html>, (Lack et al. 2015)), consist-
190 ing of the Drosophila Population Genomics Project phases 1–3 (Langley et al. 2012; Pool
191 et al. 2012), and additional African genomes (Lack et al. 2015). After removing 20 genomes
192 with more than 8% missing data, we were left with 380 samples from 16 countries across
193 Africa and Europe. Since the *Drosophila* samples are from inbred lines or haploid embryos,
194 we treat the samples as haploid when recoding; regions with residual heterozygosity were
195 marked as missing in the original dataset; we also removed positions with more than 20%
196 missing data. Each chromosome arm we investigated (X, 2L, 2R, 3L, and 3R) has 2–3
197 million SNPs; PCA plots for each arm are shown in Figure S2.

198 **Human:** We also used genomic data from the entire POPRES dataset (Nelson et al.
199 2008), which has array-derived genotype information for 447,267 SNPs across the 22 au-
200 tosomes of 3,965 samples in total: 346 African-Americans, 73 Asians, 3,187 Europeans
201 and 359 Indian Asians. Since these data derive from genotyping arrays, the SNP density is
202 much lower than the other datasets, which are each derived from whole genome sequencing.
203 We excluded the sex chromosomes and the mitochondria. PCA plots for each chromosome,
204 separately, are shown in Figure S3.

205 ***Medicago truncatula:*** Finally, we used whole-genome sequencing data from the *Med-*
206 *icago truncatula* Hapmap Project (Tang et al. 2014), which has 263 samples from 24 coun-
207 tries, primarily distributed around the Mediterranean basin. Each of the 8 chromosomes
208 has 3–5 million SNPs; PCA plots for these are shown in Figure S4. We did not use the
209 mitochondria or chloroplasts.

210 2.5 Data access

211 The methods described here are implemented in an open-source R package available at
212 https://github.com/petrelharp/local_pca, as well as scripts to perform all analyses
213 from VCF files at various parameter settings.

214 Datasets are available as follows: human (POPRES) at dbGaP with accession number
215 phs000145.v4.p2, *Medicago* at the *Medicago* Hapmap <http://www.medicagohapmap.org/>,

species	# SNPs per window	mean window length (bp)	mean # windows per chromosome	mean % variance explained by top 2 PCs
<i>Drosophila melanogaster</i>	1,000	9,019	2,674	0.53
Human	100	636,494	203	0.55
<i>Medicago truncatula</i>	10,000	102,580	467	0.50

Table 1: Descriptive statistics for each dataset used. Columns 2–4 give statistics describing the window sizes used for most analyses for each dataset (windows had a fixed number of SNPs). The final column gives the percent variance explained by the top two principal components, averaged across independent PCA of each window.

and *Drosophila* at the Drosophila Genome Nexus, <http://www.johnpool.net/genomes.html>.

3 Results

In all three datasets: a worldwide sample of humans, African *Drosophila melanogaster*, and a rangewide sample of *Medicago truncatula*, PCA plots vary along the genome in a systematic way, showing strong chromosome-scale correlations. This implies that variation is due to meaningful heterogeneity in a biological process, since noise due to randomness in choice of local genealogical trees is not expected to show long distance correlations. Below, we discuss the results and likely underlying causes.

3.1 *Drosophila melanogaster*

We applied the method to windows of average length 9 Kbp, across chromosome arms 2L, 2R, 3L, 3R and X separately. The first column of Figure 2 is a multidimensional scaling (MDS) visualization of the matrix of dissimilarities between genomic windows: in other words, genomic windows that are closer to each other in the MDS plot show more similar patterns of relatedness. For each chromosome arm, the MDS visualization roughly resembles a triangle, sometimes with additional points. Since the relative position of each window in this plot shows the similarity between windows, this suggests that there are at least three extreme manifestations of population structure typified by windows found in the “corners” of the figure, and that other windows’ patterns of relatedness may be a mixture of those extremes. The next two columns of Figure 2 respectively depict the two MDS coordinates of each window, plotted against the window’s position along the genome, to show how the plot of the first column is laid out along the genome.

To help visualize how clustered windows with similar patterns of relatedness are along each chromosome arm, we selected three “extreme” windows in the MDS plot and the 5%

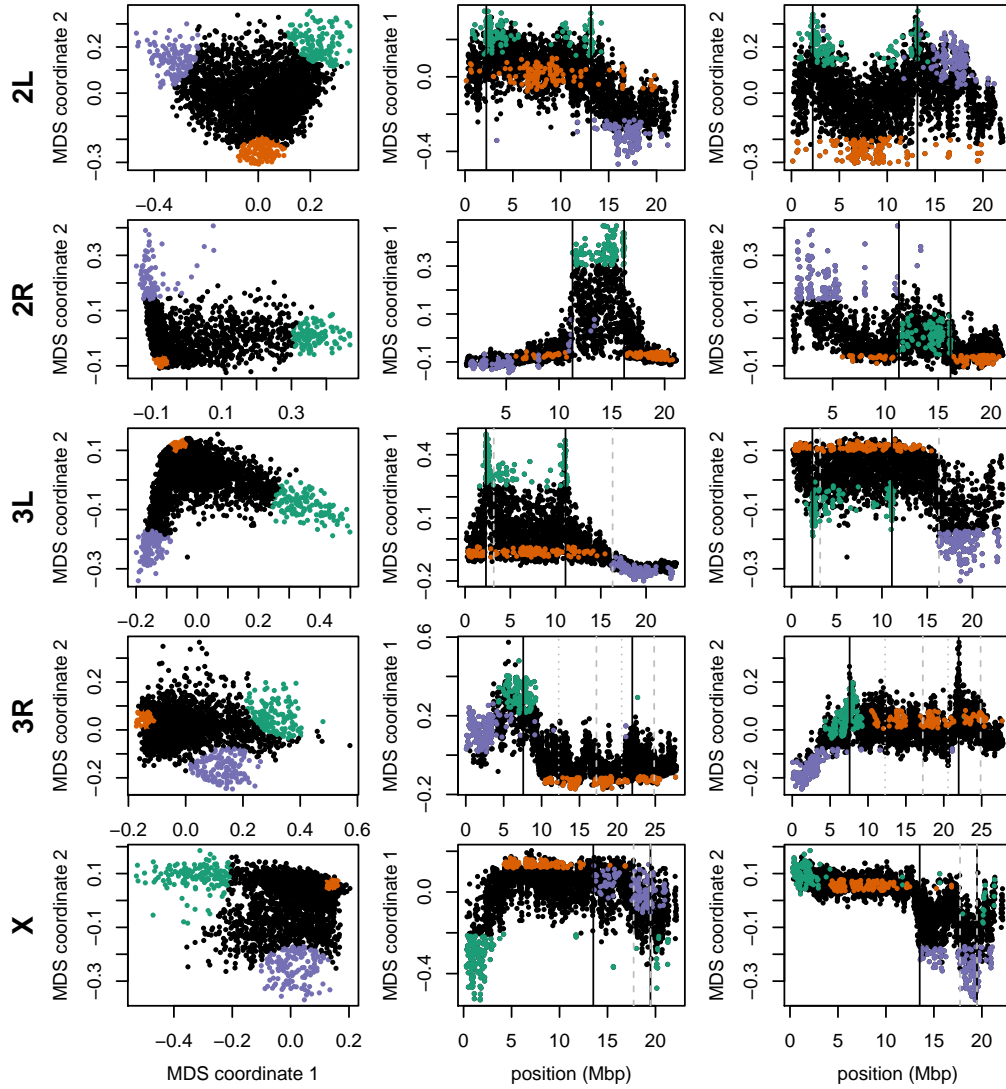


Figure 2: Variation in patterns of relatedness for windows across *Drosophila melanogaster* chromosome arms. In all plots, each point represents one window along the genome. The first column shows the MDS visualization of relationships between windows, and the second and third columns show the two MDS coordinates against the midpoint of each window; rows correspond to chromosome arms. Colors are consistent for plots in each row. Vertical lines show the breakpoints of known polymorphic inversions. Solid black lines are for the inversions we used in Figure 3, while dotted grey lines are for other known inversions.

of windows that are closest to it in the MDS coordinates, then highlighted these windows' positions along the genome, and created PCA plots for the windows, combined. Representative plots are shown for three groups of windows on each chromosome arm in Figure 2 (groups are shown in color), and in Supplemental Figure S1 (PCA plots). The latter plots are quite different, showing that genomic windows in different regions of the MDS plot indeed show quite different patterns of relatedness.

The most striking variation in patterns of relatedness turns out to be explained by several large inversions that are polymorphic in these samples, discussed in Corbett-Detig and Hartl (2012) and Langley et al. (2012). To depict this, Figure 3 shows the PCA plots in Figure S1 recolored by the orientation of the inversion for each sample. Taking chromosome arm 2L as an example, the two regions of similar, extreme patterns of relatedness shown in green in the first row of Figure 2 lie directly around the breakpoints of the inversion In(2L)t, and the PCA plots in the first rows of Figure 3 shows that patterns of relatedness here are mostly determined by inversion orientation. The regions shown in purple on chromosome 2L lie near the centromere, and have patterns of relatedness reflective of two axes of variation, seen in Figures S1 and 3, which correspond roughly to latitude within Africa and to degree of cosmopolitan admixture respectively (see Lack et al. (2015) for more about admixture in this sample). The regions shown in orange on chromosome 2L mostly lie inside the inversion, and show patterns of relatedness that are a mixture between the other two, as expected due to recombination within the (long) inversion (Guerrero et al. 2011). Similar results are found in other chromosome arms, albeit complicated by the coexistence of more than one polymorphic inversion; however, each breakpoint visibly affects patterns in the MDS coordinates (see vertical lines in Figure 2).

To see how patterns of relatedness vary in the absence of polymorphic inversions, we performed the same analyses after removing, for each chromosome arm, any samples carrying inversions on that arm. In the result, shown in Supplemental Figure S5, the striking peaks associated with inversion breakpoints are gone, and previously smaller-scale variation now dominates the MDS visualization. For instance, the majority of the variation along 3L in Figure 2 is on the left end of the arm, dominated by two large peaks around the inversion breakpoints; there is also a relatively small dip on the right end of the arm (near the centromere). In contrast, Supplemental Figure S5 shows that after removing polymorphic inversions, remaining structure is dominated by the dip near the centromere. Without inversions, variation in patterns of relatedness shown in the MDS plots follows similar patterns to that previously seen in *D. melanogaster* recombination rate and diversity (Langley et al. 2012; Mackay et al. 2012). Indeed, correlations between the recombination rate in each window and the position on the first MDS coordinate are highly significant (Spearman's $\rho = 0.54$, $p < 2 \times 10^{-16}$; Figures 4 and S6). This is consistent with the hypothesis that variation is due to selection, since the strength of linked selection increases with local gene density, measured in units of recombination distance. The number of genes – measured as the number of transcription start and end sites within each window – was not significantly correlated with MDS coordinate ($p = 0.22$).

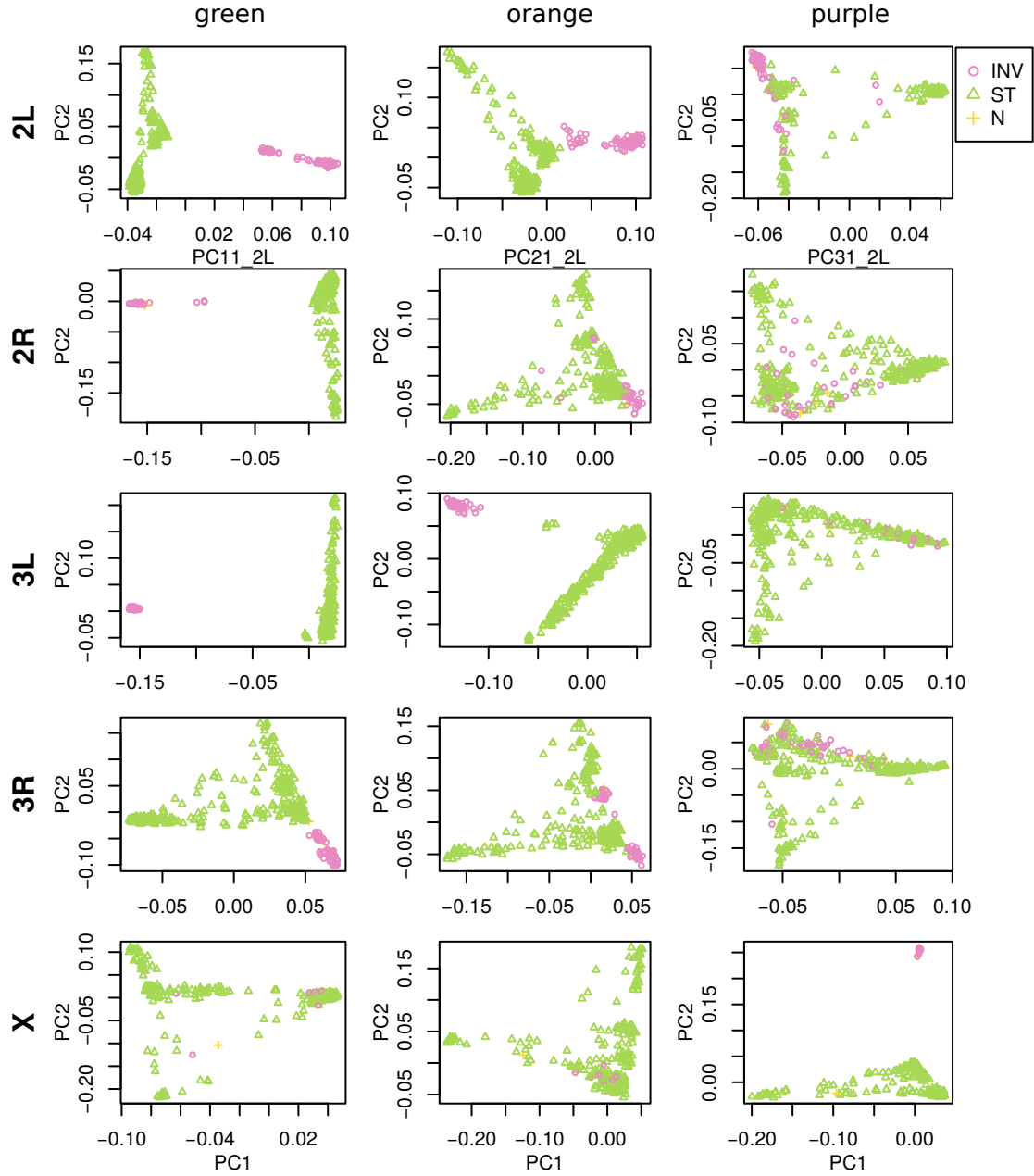


Figure 3: PCA plots for the three sets of genomic windows colored in Figure 2, on each chromosome arm of *Drosophila melanogaster*. In all plots, each point represents a sample. The first column shows the combined PCA plot for windows whose points are colored green in Figure 2; the second is for orange windows; and third is for purple windows. In each, samples are colored by orientation of the polymorphic inversions In(2L)t, In(2R)NS, In(3L)OK, In(3R)K and In(1)A respectively (data from (Lack et al. 2015)). In each “INV” denotes an inverted genotype, “ST” denotes the standard orientation, and “N” denotes unknown.

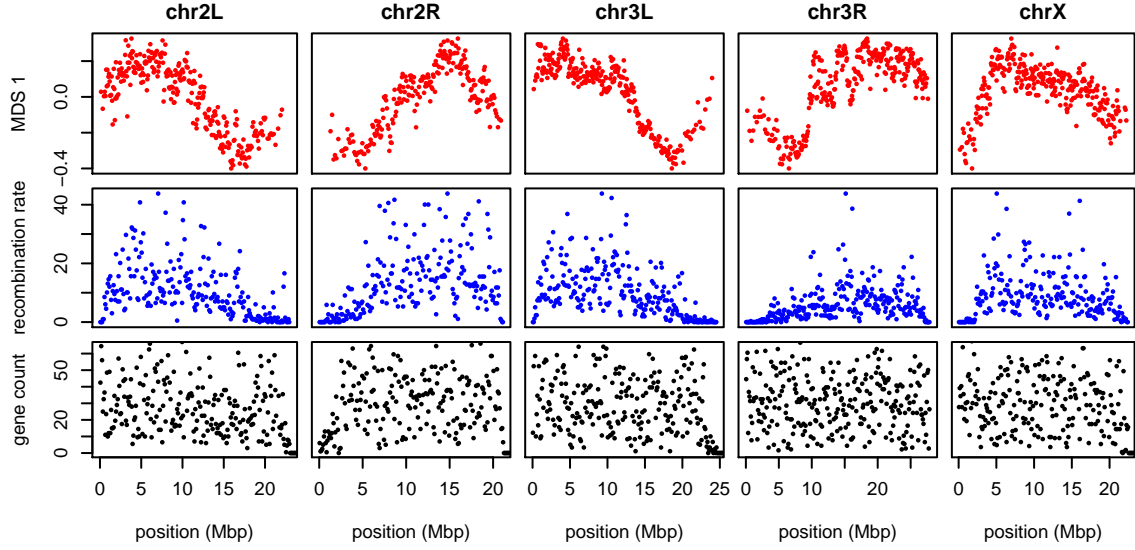


Figure 4: The effects of population structure without inversions is correlated to recombination rate in *Drosophila melanogaster*. The first plot (in red) shows the first MDS coordinate along the genome for windows of 10,000 SNPs, obtained after removing samples with inversions. (A plot analogous to Figure 2 is shown in Supplemental Figure S5.) The second plot (in blue) shows local average recombination rates in cM/Mbp, obtained as midpoint estimates for 100Kbp windows from the *Drosophila* recombination rate calculator (Fiston-Lavier et al. 2010) release 5, using rates from Comeron et al. (2012). The third plot (in black) shows the number of genes' transcription start and end sites within each 100Kbp window, divided by two. Transcription start and end sites were obtained from the RefGene table from the UCSC browser. The histone gene cluster on chromosome arm 2L is excluded.

3.2 Human

As we did for the *Drosophila* data, we applied our method separately to all 22 human autosomes. On each, variation in patterns of relatedness was dominated by a small number of windows having similar patterns of relatedness to each other that differed dramatically from the rest of the chromosome. These may be primarily inversions: outlying windows coincide with three of the six large polymorphic inversions described in Antonacci et al. (2009), notably a particularly large, polymorphic inversion on 8p23 (Figure 5). Similar plots for all chromosomes are shown in Supplementary Figures S7, S8, and S9. PCA plots of many outlying windows show a characteristic trimodal shape (shown for chromosome 8 in Figure S10), presumably distinguishing samples having each of the three diploid genotypes for each inversion orientation (although we do not have data on orientation status). This trimodal shape has been proposed as a method to identify inversions (Ma and Amos 2012), but distinguishing this hypothesis from others, such as regions of low recombination rate, would require additional data.

We also applied the method on all 22 autosomes together, and found that, remarkably, the inversion on chromosome 8 is still the most striking outlying signal (Figure S11). Further investigation with a denser set of SNPs, allowing a finer genomic resolution, may yield other patterns.

3.3 *Medicago truncatula*

Unlike the other two species, the method applied separately on all eight chromosomes of *Medicago truncatula* showed similar patterns of gradual change in patterns of relatedness across each chromosome, with no indications of chromosome-specific patterns. This consistency suggests that the factor affecting the population structure for each chromosome is the same, as might be caused by varying strengths of linked selection. To verify that variation in the effects of population structure is shared across chromosomes, we applied the method to all chromosomes together. Results for chromosome 3 are shown in Figures 6 and 6, and other chromosomes are similar: across chromosomes, the high values of the first MDS coordinate coincide with the position of the heterochromatic regions surrounding the centromere, which often have lower gene density and may therefore be less subject to linked selection. To verify that this is a possible explanation, we counted the number of genes found in each window using gene models in Mt4.0 from jcvi.org (Tang et al. 2014), which are shown juxtaposed with the first MDS coordinate of each window in Figure 7, and are significantly correlated, as shown in Supplemental Figure S12. (Values shown are the number of start and end positions of each predicted mRNA transcript, divided by two, assigned to the nearest window.) However, other genomic features, such as distance to centromere show roughly the same patterns, so we cannot rule out alternative hypotheses. In particular, the recombination rates estimated by Paape et al. (2012) appear visually to be similar, but were not available in a form that can be compared to our MDS values.

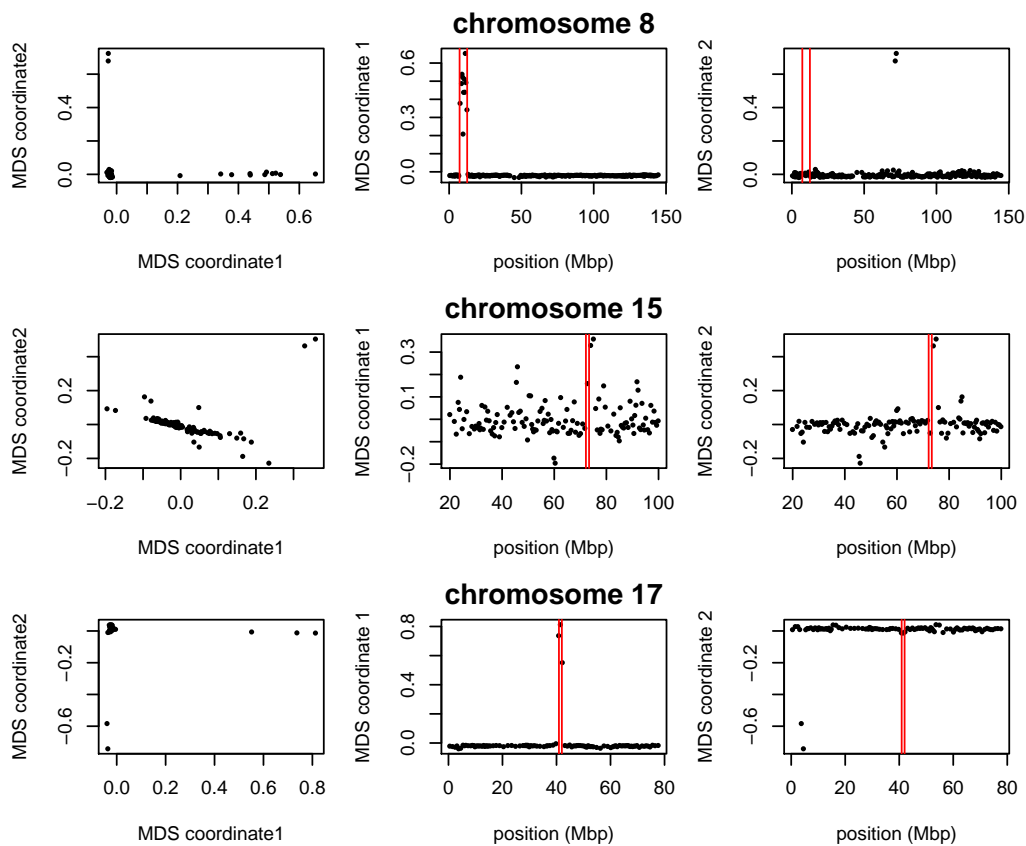


Figure 5: Variation in structure between windows on human chromosomes 8, 15, and 17. Each point in each plot represents a window. The first column shows the MDS visualization of relationships between windows; the second and third columns show the two MDS coordinates of each window against its position (midpoint) along the chromosome. Rows, from top to bottom show chromosomes 8, 15, and 17. The vertical red lines show the breakpoints of known inversions from Antonacci et al. (2009).

319 We also found nearly identical results when choosing shorter windows of 1,000 SNPs;
320 or choosing windows of equal length in base pairs rather than SNPs. Similarly, the results
321 were not substantially changed when using weighted PCA to downweight the large group
322 of Tunisian samples.

323 4 Discussion

324 Our investigations have found substantial variation in the patterns of relatedness formed
325 by population structure across the genomes of three diverse species, revealing distinct bi-
326 ological processes driving this variation in each species. More investigation, particularly
327 on more species and datasets, will help to uncover what aspects of species history can
328 explain these differences. With growing appreciation of the heterogeneous effects of se-
329 lection across the genome, especially the importance of adaptive introgression and hybrid
330 speciation (Brandvain et al. 2014; Fitzpatrick et al. 2010; Hufford et al. 2013; Pool 2015;
331 Staubach et al. 2012), local adaptation (Lenormand 2002; Wang and Bradburd 2014), and
332 inversion polymorphisms (Kirkpatrick 2010; Kirkpatrick and Barrett 2015), local PCA may
333 prove to be a useful exploratory tool to discover important genomic features.

334 We now discuss possible implications of this variation in the effects of population struc-
335 ture, the impact of various parameter choices in implementing the method, and possible
336 additional applications.

337 **Chromosomal inversions** A major driver of variation in patterns of relatedness in
338 two datasets we examined are inversions. This may be common, but the example of
339 *Medicago truncatula* shows that polymorphic inversions are not ubiquitous. PCA has been
340 proposed as a method for discovering inversions (Ma and Amos 2012); however, the signal
341 left by inversions likely cannot be distinguished from long haplotypes under balancing
342 selection or simply regions of reduced recombination without additional lines of evidence.
343 Inversions show up in our method because across the inverted region, most gene trees
344 share a common split that dates back to the origin of the inversion. However, in many
345 applications, inversions are a nuisance. For instance, SMARTPCA (Patterson et al. 2006)
346 reduces their effect on PCA plots by regressing out the effect of linked SNPs on each
347 other. Removing samples with the less common orientation of each inversion reduced, but
348 did not eliminate, the signal of inversions seen in the *Drosophila melanogaster* dataset,
349 demonstrating that the genomic effects of transiently polymorphic inversions may outlast
350 the inversions themselves.

351 **The effect of selection** It seems that the variation in patterns of relatedness we see in
352 the *Medicago truncatula* and *Drosophila melanogaster* datasets must be explained some-
353 how by linked selection. Furthermore, the selection must be affecting many targets across
354 the genome, since we see similar effects across long distances (even distinct chromosomes).

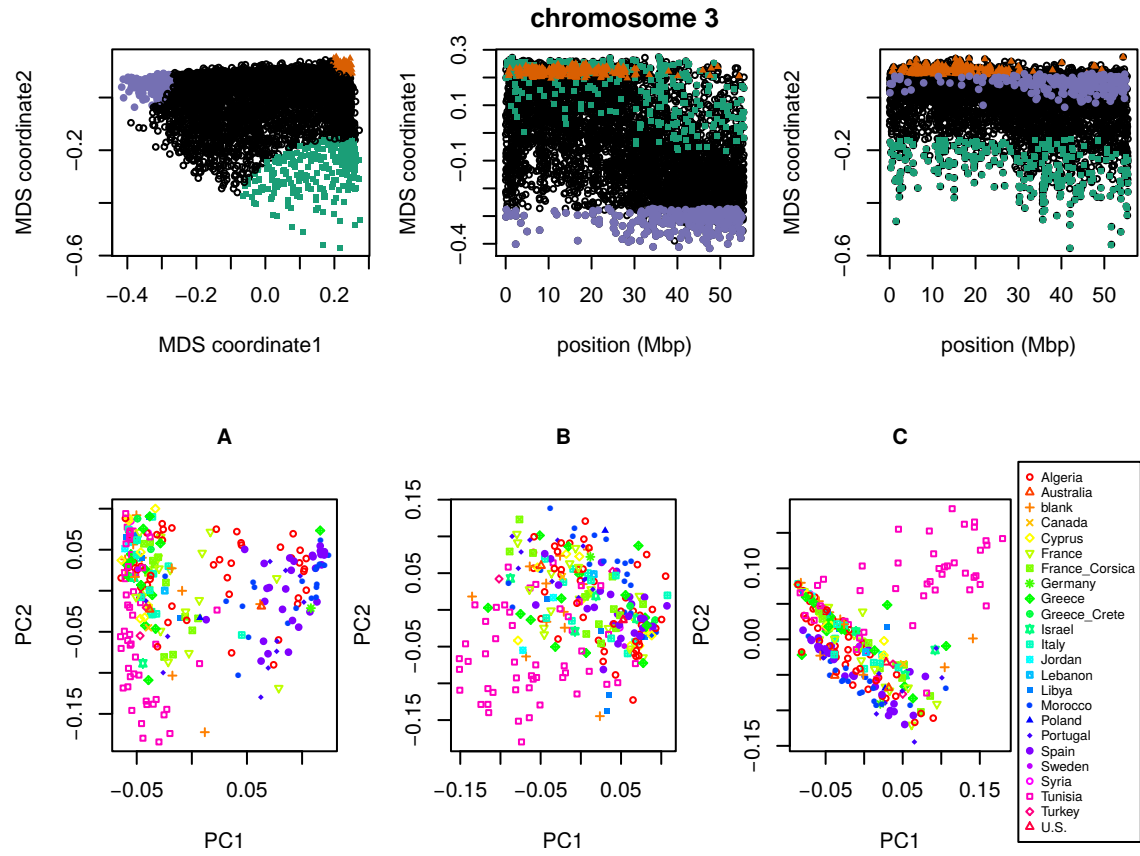


Figure 6: MDS visualization of patterns of relatedness on *M. truncatula* chromosome 3, with corresponding PCA plots. Each point in the plot represents a window; the structure revealed by the MDS plot is strongly clustered along the chromosome, with windows in the upper-right corner of the MDS plot (colored red) clustered around the centromere, windows in the upper-left corner (purple) furthest from the centromere, and the remaining corner (green) intermediate. Plots for remaining chromosomes are shown in Supplemental Figure S13. **(below)** PCA plots for the sets of genomic windows colored (A) green, (B) orange, and (C) purple in Figure 6. Each point corresponds to a sample, colored by country of origin. Plots for remaining chromosomes are shown in Supplemental Figure S14.

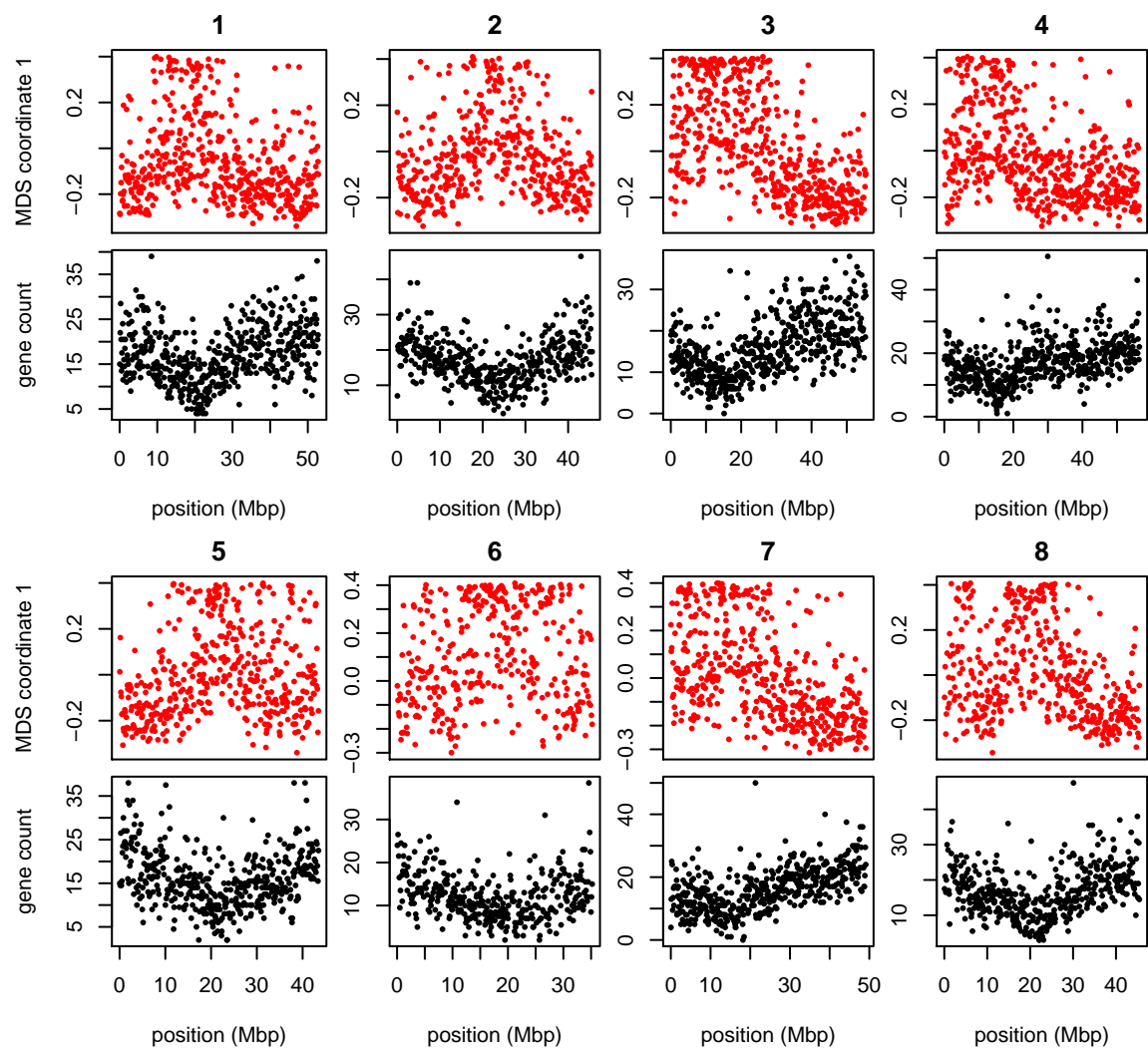


Figure 7: MDS coordinate and gene density for each window in the *Medicago* genome, for chromosomes 1–8 (numbered above each pair of figures). For each chromosome, the red plot above is first coordinate of MDS against the middle position of each window along each chromosome. The black plot below is gene count for each window against the position of each window.

355 For this reason, the most likely candidate may be selection against linked deleterious mu-
 356 tations, known as “background selection” (Charlesworth et al. 1993; Charlesworth 2013).
 357 Informally, background selection reduces the number of potential contributors to the gene
 358 pool in regions of the genome with many possible deleterious mutations (Hudson and Ka-
 359 plan 1995); for this reason, if it acts in a spatial context, it is expected to induce samples
 360 from nearby locations to cluster together more frequently. Therefore, regions of the genome
 361 harboring many targets of local adaptation may show similar patterns, since migrant alleles
 362 in these regions will be selected against, and so locally gene trees will more closely reflect
 363 spatial proximity.

364 A related possibility is that variation in patterns of relatedness is due to recent ad-
 365 mixture between previously separated populations, the effects of which were not uniform
 366 across the genome due to selection. For instance, it has been hypothesized that large-scale
 367 variation in amount of introgressed Neanderthal DNA along the genome is due to selection
 368 against Neanderthal genes, leading to greater introgression in regions of lower gene density
 369 (Harris and Nielsen 2016; Juric et al. 2016). African *Drosophila melanogaster* are known to
 370 have a substantial amount of recently introgressed genome from “cosmopolitan” sources;
 371 if selection regularly favors genes from one origin, this could lead to substantial variation
 372 in patterns of relatedness correlated with local gene density.

373 There has been substantial debate over the relative impacts of different forms of se-
 374 lection. These have been difficult to disentangle in part because for the most part theory
 375 makes predictions which are only strictly valid in randomly mating (i.e., unstructured)
 376 populations, and it is unclear to what extent the spatial structure observed in most real
 377 populations will affect these predictions. It may be possible to design more powerful statis-
 378 tics that make stronger use of spatial information.

379 **Parameter choices** There are several choices in the method that may in principle affect
 380 the results. As with whole-genome PCA, the choice of samples is important, as variation
 381 not strongly represented in the sample will not be discovered. The effects of strongly
 382 imbalanced sampling schemes are often corrected by dropping samples in overrepresented
 383 groups; but downweighting may be a better option that does not discard data (and here we
 384 present a method to do this). Next, the choice of window size may be important, although
 385 in our applications results were not sensitive to this, indicating that we can see variation
 386 on a sufficiently fine scale. Finally, which collections of genomic regions are compared to
 387 each other (steps 3 and 4 in Figure 1), along with the method used to discover common
 388 structure, will affect results. We used MDS, applied to either each chromosome separately
 389 or to the entire genome; for instance, human inversions are clearly visible as outliers when
 390 compared to the rest of their chromosome, but genome-wide, their signal is obscured by
 391 the numerous other signals of comparable strength.

392 Besides window length, there is also the question of how to choose windows. In these
 393 applications we have used nonoverlapping windows with equal numbers of polymorphic
 394 sites. Alternatively, windows could be chosen to have equal length in genetic distance, so

395 that each would have roughly the same number of independent trees. However, we found
396 little change in results when using different window sizes or when measuring windows in
397 physical distance (in bp).

398 Finally, our software allows different choices for how many PCs to use in approximating
399 structure of each window (k in equation 1), and how many MDS coordinates to use when
400 describing the distance matrix between windows, but in our exploration, changing these has
401 not produced dramatically different results. These are all part of more general techniques
402 in dimension reduction and high-dimensional data visualization; we encourage the user to
403 experiment.

404 **Applications** So-called cryptic relatedness between samples has been one of the major
405 sources of confounding in genome-wide association studies (GWAS) and so methods must
406 account for it by modeling population structure or kinship (Aste and Balding 2009; Yang
407 et al. 2014). Since the effects of population structure is not constant along the genome, this
408 could in principle lead to an inflation of false positives in parts of the genome with stronger
409 population structure than the genome-wide average. A method such as ours might be used
410 to provide a more sensitive correction. Fortunately, in our human dataset this does not
411 seem likely to have a strong effect: most variation is due to small, independent regions,
412 possibly primarily inversions, and so may not have a major effect on GWAS. In the other
413 species we examined, particularly *Drosophila melanogaster*, treating population structure
414 as a single quantity would entail a substantial loss of power, and could potentially be
415 misleading.

416 Acknowledgements

417 We are indebted to John Pool, Russ Corbett-Detig, Matilde Cordeiro, and Peter Chang
418 for assistance with obtaining data and interpreting results (especially inversion status of
419 *D. melanogaster* samples). Jaime Ashander and Jerome Kelleher provided assistance in
420 performing the simulations. Thanks also go to Yaniv Brandvain, Barbara Engelhardt,
421 Charles Langley, Graham Coop, and Jeremy Berg for helpful comments and for encouraging
422 the project.

423 Disclosure declaration

424 The authors declare no conflicts of interest.

References

- Francesca Antonacci, Jeffrey M Kidd, Tomas Marques-Bonet, Mario Ventura, Priscillia Siswara, Zhaoshi Jiang, and Evan E Eichler. Characterization of six human disease-associated inversion polymorphisms. *Human molecular genetics*, 18(14):2555–2566, 2009.
- William Astle and David J. Balding. Population structure and cryptic relatedness in genetic association studies. *Statistical Science*, 24(4):451–471, 11 2009. doi: 10.1214/09-STS307. URL <http://dx.doi.org/10.1214/09-STS307>.
- Nicholas H. Barton. Genetic hitchhiking. *Philos Trans R Soc Lond B Biol Sci*, 355(1403):1553–1562, November 2000. doi: 10.1098/rstb.2000.0716. URL <http://www.ncbi.nlm.nih.gov/pmc/articles/PMC1692896/>.
- Albert P. Blair. Population structure in toads. *The American Naturalist*, 77(773):563–568, 1943. ISSN 00030147, 15375323. URL <http://www.jstor.org/stable/2457848>.
- Yaniv Brandvain, Amanda M. Kenney, Lex Flagel, Graham Coop, and Andrea L. Sweigart. Speciation and introgression between *Mimulus nasutus* and *Mimulus guttatus*. *PLoS Genet*, 10(6):e1004410, 06 2014. doi: 10.1371/journal.pgen.1004410. URL <http://dx.doi.org/10.1371/journal.pgen.1004410>.
- Frank M.T.A. Busing, Erik Meijer, and Rien Van Der Leeden. Delete-m jackknife for unequal m. *Statistics and Computing*, 9(1):3–8, 1999. ISSN 0960-3174. doi: 10.1023/A:1008800423698. URL <http://dx.doi.org/10.1023/A%3A1008800423698>.
- B Charlesworth, M T Morgan, and D Charlesworth. The effect of deleterious mutations on neutral molecular variation. *Genetics*, 134(4):1289–1303, August 1993. URL <http://www.genetics.org/content/134/4/1289>.
- Brian Charlesworth. Background selection 20 years on: The Wilhelmine E. Key 2012 invitational lecture. *Journal of Heredity*, 104(2):161–171, 2013. doi: 10.1093/jhered/ess136. URL <http://jhered.oxfordjournals.org/content/104/2/161.abstract>.
- Brian Charlesworth, Deborah Charlesworth, and Nicholas H. Barton. The effects of genetic and geographic structure on neutral variation. *Annual Review of Ecology, Evolution, and Systematics*, 34(1):99–125, 2003. doi: 10.1146/annurev.ecolsys.34.011802.132359. URL <http://arjournals.annualreviews.org/doi/abs/10.1146/annurev.ecolsys.34.011802.132359>.
- J M Comeron, R Ratnappan, and S Bailin. The many landscapes of recombination in *Drosophila melanogaster*. *PLoS Genet*, 8(10), 2012. doi: 10.1371/journal.pgen.1002905. URL <http://www.ncbi.nlm.nih.gov/pmc/articles/PMC3469467/>.

- 458 Russell B Corbett-Detig and Daniel L Hartl. Population genomics of inversion polymor-
459 phisms in *Drosophila melanogaster*. *PLoS Genet*, 8(12):e1003056, 2012.
- 460 Nicolas Duforet-Frebourg, Keurcien Luu, Guillaume Laval, Eric Bazin, and Michael G.B.
461 Blum. Detecting genomic signatures of natural selection with principal component
462 analysis: Application to the 1000 genomes data. *Molecular Biology and Evolution*,
463 2015. doi: 10.1093/molbev/msv334. URL [http://mbe.oxfordjournals.org/content/
464 early/2016/01/12/molbev.msv334.abstract](http://mbe.oxfordjournals.org/content/early/2016/01/12/molbev.msv334.abstract).
- 465 B. Efron. *The Jackknife, the Bootstrap and Other Resampling Plans*. Society for Industrial
466 and Applied Mathematics, 1982. doi: 10.1137/1.9781611970319. URL [http://epubs.
467 siam.org/doi/abs/10.1137/1.9781611970319](http://epubs.siam.org/doi/abs/10.1137/1.9781611970319).
- 468 Hans Ellegren, Linnea Smeds, Reto Burri, Pall I. Olason, Niclas Backstrom, Takeshi
469 Kawakami, Axel Kunstner, Hannu Makinen, Krystyna Nadachowska-Brzyska, Anna
470 Qvarnstrom, Severin Uebbing, and Jochen B. W. Wolf. The genomic landscape of species
471 divergence in *Ficedula* flycatchers. *Nature*, 491(7426):756–760, November 2012. ISSN
472 00280836. doi: 10.1038/nature11584. URL <http://dx.doi.org/10.1038/nature11584>.
- 473 Barbara E. Engelhardt and Matthew Stephens. Analysis of population structure: a uni-
474 fying framework and novel methods based on sparse factor analysis. *PLoS Genet*, 6(9),
475 September 2010. doi: 10.1371/journal.pgen.1001117. URL [http://www.ncbi.nlm.nih.
476 gov/pubmed/20862358](http://www.ncbi.nlm.nih.gov/pubmed/20862358).
- 477 Anna-Sophie Fiston-Lavier, Nadia D. Singh, Mikhail Lipatov, and Dmitri A. Petrov.
478 *Drosophila melanogaster* recombination rate calculator. *Gene*, 463(1–2):18 – 20, 2010.
479 ISSN 0378-1119. doi: <http://dx.doi.org/10.1016/j.gene.2010.04.015>. URL [http://www.
480 sciencedirect.com/science/article/pii/S0378111910001769](http://www.sciencedirect.com/science/article/pii/S0378111910001769).
- 481 B M Fitzpatrick, J R Johnson, D K Kump, J J Smith, S R Voss, and H B Shaffer.
482 Rapid spread of invasive genes into a threatened native species. *Proc Natl Acad Sci*
483 *U S A*, 107(8):3606–3610, February 2010. doi: 10.1073/pnas.0911802107. URL [http:
484 //www.ncbi.nlm.nih.gov/pubmed/20133596](http://www.ncbi.nlm.nih.gov/pubmed/20133596).
- 485 Rafael F. Guerrero, François Rousset, and Mark Kirkpatrick. Coalescent patterns for
486 chromosomal inversions in divergent populations. *Philosophical Transactions of the*
487 *Royal Society B: Biological Sciences*, 367(1587):430–438, 2011. ISSN 0962-8436. doi:
488 10.1098/rstb.2011.0246. URL [http://rstb.royalsocietypublishing.org/content/
489 367/1587/430](http://rstb.royalsocietypublishing.org/content/367/1587/430).
- 490 Kelley Harris and Rasmus Nielsen. The genetic cost of Neanderthal introgression. *Genetics*,
491 203(2):881–891, June 2016. URL <http://www.genetics.org/content/203/2/881>.

492 R R Hudson and N L Kaplan. Deleterious background selection with recombination. *Ge-*
493 *netics*, 141(4):1605–1617, December 1995. URL [http://www.genetics.org/content/](http://www.genetics.org/content/141/4/1605)
494 [141/4/1605](http://www.genetics.org/content/141/4/1605).

495 Emilia Huerta-Sánchez, Michael DeGiorgio, Luca Pagani, Ayele Tarekegn, Rosemary
496 Ekong, Tiago Antao, Alexia Cardona, Hugh E. Montgomery, Gianpiero L. Cavalleri,
497 Peter A. Robbins, Michael E. Weale, Neil Bradman, Endashaw Bekele, Toomas Kivisild,
498 Chris Tyler-Smith, and Rasmus Nielsen. Genetic signatures reveal high-altitude adapta-
499 tion in a set of Ethiopian populations. *Molecular Biology and Evolution*, 30(8):1877–1888,
500 2013. doi: 10.1093/molbev/mst089. URL [http://mbe.oxfordjournals.org/content/](http://mbe.oxfordjournals.org/content/30/8/1877.abstract)
501 [30/8/1877.abstract](http://mbe.oxfordjournals.org/content/30/8/1877.abstract).

502 Matthew B. Hufford, Pesach Lubinsky, Tanja Pyhäjärvi, Michael T. Devengenzo, Nor-
503 man C. Ellstrand, and Jeffrey Ross-Ibarra. The genomic signature of crop-wild introgres-
504 sion in maize. *PLoS Genet*, 9(5):e1003477, 05 2013. doi: 10.1371/journal.pgen.1003477.
505 URL <http://dx.doi.org/10.1371%2Fjournal.pgen.1003477>.

506 Ivan Juric, Simon Aeschbacher, and Graham Coop. The strength of selection against
507 Neanderthal introgression. *bioRxiv*, 2016. doi: 10.1101/030148. URL [http://biorxiv.](http://biorxiv.org/content/early/2016/07/22/030148)
508 [org/content/early/2016/07/22/030148](http://biorxiv.org/content/early/2016/07/22/030148).

509 N. Kambhatla and T. K. Leen. Dimension reduction by local principal component analysis.
510 *Neural Computation*, 9(7):1493–1516, July 1997. ISSN 0899-7667. doi: 10.1162/neco.
511 1997.9.7.1493. URL [http://ieeexplore.ieee.org/xpl/freeabs_all.jsp?arnumber=](http://ieeexplore.ieee.org/xpl/freeabs_all.jsp?arnumber=6795533)
512 [6795533](http://ieeexplore.ieee.org/xpl/freeabs_all.jsp?arnumber=6795533).

513 Yuseob Kim and Wolfgang Stephan. Detecting a local signature of genetic hitchhiking
514 along a recombining chromosome. *Genetics*, 160(2):765–777, 2002. URL [http://www.](http://www.genetics.org/cgi/content/abstract/160/2/765)
515 [genetics.org/cgi/content/abstract/160/2/765](http://www.genetics.org/cgi/content/abstract/160/2/765).

516 Mark Kirkpatrick. How and why chromosome inversions evolve. *PLoS Biol*, 8(9), 2010.
517 doi: 10.1371/journal.pbio.1000501. URL [http://www.ncbi.nlm.nih.gov/pubmed/](http://www.ncbi.nlm.nih.gov/pubmed/20927412)
518 [20927412](http://www.ncbi.nlm.nih.gov/pubmed/20927412).

519 Mark Kirkpatrick and Brian Barrett. Chromosome inversions, adaptive cassettes and the
520 evolution of species’ ranges. *Molecular Ecology*, 2015. ISSN 1365-294X. doi: 10.1111/
521 [mec.13074](http://dx.doi.org/10.1111/mec.13074). URL <http://dx.doi.org/10.1111/mec.13074>.

522 Justin B Lack, Charis M Cardeno, Marc W Crepeau, William Taylor, Russell B Corbett-
523 Detig, Kristian A Stevens, Charles H Langley, and John E Pool. The *Drosophila* genome
524 nexus: a population genomic resource of 623 *Drosophila melanogaster* genomes, including
525 197 from a single ancestral range population. *Genetics*, 199(4):1229–1241, 2015.

526 C H Langley, K Stevens, C Cardeno, Y C Lee, D R Schrider, J E Pool, S A Langley,
527 C Suarez, R B Corbett-Detig, B Kolaczowski, S Fang, P M Nista, A K Holloway, A D
528 Kern, C N Dewey, Y S Song, M W Hahn, and D J Begun. Genomic variation in natural
529 populations of *Drosophila melanogaster*. *Genetics*, 192(2):533–598, October 2012. doi:
530 10.1534/genetics.112.142018. URL <http://www.ncbi.nlm.nih.gov/pubmed/22673804>.

531 Thomas Lenormand. Gene flow and the limits to natural selection. *Trends in Ecol-*
532 *ogy & Evolution*, 17(4):183 – 189, 2002. ISSN 0169-5347. doi: DOI:10.1016/
533 S0169-5347(02)02497-7. URL [http://www.sciencedirect.com/science/article/](http://www.sciencedirect.com/science/article/pii/S0169534702024977)
534 [pii/S0169534702024977](http://www.sciencedirect.com/science/article/pii/S0169534702024977).

535 J Ma and C I Amos. Investigation of inversion polymorphisms in the human genome
536 using principal components analysis. *PLoS One*, 7(7), 2012. doi: 10.1371/journal.pone.
537 0040224. URL <http://www.ncbi.nlm.nih.gov/pubmed/22808122>.

538 Trudy F. C. Mackay, Stephen Richards, Eric A. Stone, Antonio Barbadilla, Julien F.
539 Ayroles, Dianhui Zhu, Sonia Casillas, Yi Han, Michael M. Magwire, Julie M. Crid-
540 land, Mark F. Richardson, Robert R. H. Anholt, Maite Barron, Crystal Bess, Ker-
541 stin Petra Blankenburg, Mary Anna Carbone, David Castellano, Lesley Chaboub, Laura
542 Duncan, Zeke Harris, Mehwish Javaid, Joy Christina Jayaseelan, Shalini N. Jhangiani,
543 Katherine W. Jordan, Fremiet Lara, Faye Lawrence, Sandra L. Lee, Pablo Librado,
544 Raquel S. Linheiro, Richard F. Lyman, Aaron J. Mackey, Mala Munidasa, Donna Marie
545 Muzny, Lynne Nazareth, Irene Newsham, Lora Perales, Ling-Ling Pu, Carson Qu, Miquel
546 Ramia, Jeffrey G. Reid, Stephanie M. Rollmann, Julio Rozas, Nehad Saada, Lavanya
547 Turlapati, Kim C. Worley, Yuan-Qing Wu, Akihiko Yamamoto, Yiming Zhu, Casey M.
548 Bergman, Kevin R. Thornton, David Mittelman, and Richard A. Gibbs. The *Drosophila*
549 *melanogaster* genetic reference panel. *Nature*, 482(7384):173–178, February 2012. ISSN
550 00280836. URL <http://dx.doi.org/10.1038/nature10811>.

551 José V Manjón, Pierrick Coupé, Luis Concha, Antonio Buades, D Louis Collins, and
552 Montserrat Robles. Diffusion weighted image denoising using overcomplete local PCA.
553 *PloS one*, 8(9):e73021, 2013.

554 Simon Henry Martin, Markus Moest, Wiliam J Palmer, Camilo Salazar, W. Owen McMil-
555 lan, Francis M Jiggins, and Chris D Jiggins. Natural selection and genetic diversity
556 in the butterfly *Heliconius melpomene*. *Genetics*, 203(1):525–541, May 2016. doi:
557 10.1101/042796. URL <http://www.genetics.org/content/203/1/525>.

558 Gil McVean. A genealogical interpretation of principal components analysis. *PLoS Genet*,
559 5(10):e1000686, 2009.

560 P Menozzi, A Piazza, and L Cavalli-Sforza. Synthetic maps of human gene frequencies in
561 Europeans. *Science*, 201(4358):786–792, September 1978. URL [http://www.ncbi.nlm.](http://www.ncbi.nlm.nih.gov/pubmed/356262)
562 [nih.gov/pubmed/356262](http://www.ncbi.nlm.nih.gov/pubmed/356262).

563 N J Nadeau, A Whibley, R T Jones, J W Davey, K K Dasmahapatra, S W Baxter,
564 M A Quail, M Joron, R H French Constant, M L Blaxter, J Mallet, and C D Jiggins.
565 Genomic islands of divergence in hybridizing *Heliconius* butterflies identified by large-
566 scale targeted sequencing. *Philos Trans R Soc Lond B Biol Sci*, 367(1587):343–353,
567 February 2012. doi: 10.1098/rstb.2011.0198. URL [http://www.ncbi.nlm.nih.gov/
568 pubmed/22201164](http://www.ncbi.nlm.nih.gov/pubmed/22201164).

569 M R Nelson, K Bryc, K S King, A Indap, A R Boyko, J Novembre, L P Briley, Y Maruyama,
570 D M Waterworth, G Waeber, P Vollenweider, J R Oksenberg, S L Hauser, H A Stirnadel,
571 J S Kooner, J C Chambers, B Jones, V Mooser, C D Bustamante, A D Roses, D K Burns,
572 M G Ehm, and E H Lai. The Population Reference Sample, POPRES: a resource for
573 population, disease, and pharmacological genetics research. *Am J Hum Genet*, 83(3):
574 347–358, September 2008. doi: 10.1016/j.ajhg.2008.08.005. URL [http://www.ncbi.
575 nlm.nih.gov/pmc/articles/PMC2556436/?tool=pubmed](http://www.ncbi.nlm.nih.gov/pmc/articles/PMC2556436/?tool=pubmed).

576 John Novembre and Matthew Stephens. Interpreting principal component analyses of
577 spatial population genetic variation. *Nature genetics*, 40(5):646–649, 2008.

578 John Novembre, Toby Johnson, Katarzyna Bryc, Zoltán Kutalik, Adam R Boyko, Adam
579 Auton, Amit Indap, Karen S King, Sven Bergmann, Matthew R Nelson, et al. Genes
580 mirror geography within europe. *Nature*, 456(7218):98–101, 2008.

581 Timothy Paape, Peng Zhou, Antoine Branca, Roman Briskine, Nevin Young, and Peter
582 Tiffin. Fine-scale population recombination rates, hotspots, and correlates of recombina-
583 tion in the *Medicago truncatula* genome. *Genome Biology and Evolution*, 4(5):726–737,
584 2012. doi: 10.1093/gbe/evs046. URL [http://gbe.oxfordjournals.org/content/4/
585 5/726.abstract](http://gbe.oxfordjournals.org/content/4/5/726.abstract).

586 Nick Patterson, Alkes L Price, and David Reich. Population structure and eigenanalysis.
587 *PLoS Genetics*, 2(12):e190, 12 2006. doi: 10.1371/journal.pgen.0020190. URL [http:
588 //dx.plos.org/10.1371%2Fjournal.pgen.0020190](http://dx.plos.org/10.1371%2Fjournal.pgen.0020190).

589 J B Pease and M W Hahn. More accurate phylogenies inferred from low-recombination
590 regions in the presence of incomplete lineage sorting. *Evolution*, 67(8):2376–2384, August
591 2013. doi: 10.1111/evo.12118. URL <http://www.ncbi.nlm.nih.gov/pubmed/23888858>.

592 John E Pool. The mosaic ancestry of the *Drosophila* Genetic Reference Panel and the
593 *D. melanogaster* reference genome reveals a network of epistatic fitness interactions.
594 *Molecular Biology and Evolution*, 32(12):3236–3251, 2015. doi: 10.1101/014837. URL
595 <http://mbe.oxfordjournals.org/content/32/12/3236.abstract>.

596 John E. Pool, Russell B. Corbett-Detig, Ryuichi P. Sugino, Kristian A. Stevens, Charis M.
597 Cardeno, Marc W. Crepeau, Pablo Duchon, J. J. Emerson, Perot Saelao, David J. Begun,
598 and Charles H. Langley. Population genomics of sub-Saharan *Drosophila melanogaster*:

599 African diversity and non-African admixture. *PLoS Genet*, 8(12):1–24, 12 2012. doi:
600 10.1371/journal.pgen.1003080. URL [http://dx.doi.org/10.1371%2Fjournal.pgen.](http://dx.doi.org/10.1371%2Fjournal.pgen.1003080)
601 1003080.

602 Alkes L Price, Nick J Patterson, Robert M Plenge, Michael E Weinblatt, Nancy A Shadick,
603 and David Reich. Principal components analysis corrects for stratification in genome-
604 wide association studies. *Nature genetics*, 38(8):904–909, 2006.

605 Yixuan Qiu and Jiali Mei. *RSpectra: Solvers for Large Scale Eigenvalue and SVD Problems*,
606 2016. URL <https://CRAN.R-project.org/package=RSpectra>. R package version 0.11-
607 0.

608 Sam T. Roweis and Lawrence K. Saul. Nonlinear dimensionality reduction by locally linear
609 embedding. *Science*, 290(5500):2323–2326, 2000. ISSN 0036-8075. doi: 10.1126/science.
610 290.5500.2323. URL <http://science.sciencemag.org/content/290/5500/2323>.

611 Fabian Staubach, Anna Lorenc, Philipp W. Messer, Kun Tang, Dmitri A. Petrov, and
612 Diethard Tautz. Genome patterns of selection and introgression of haplotypes in natural
613 populations of the house mouse (*Mus musculus*). *PLoS Genet*, 8(8):e1002891, 08 2012.
614 doi: 10.1371/journal.pgen.1002891. URL [http://dx.doi.org/10.1371%2Fjournal.](http://dx.doi.org/10.1371%2Fjournal.pgen.1002891)
615 [pgen.1002891](http://dx.doi.org/10.1371%2Fjournal.pgen.1002891).

616 Haibao Tang, Vivek Krishnakumar, Shelby Bidwell, Benjamin Rosen, Agnes Chan, Shiguo
617 Zhou, Laurent Gentzbittel, Kevin L Childs, Mark Yandell, Heidrun Gundlach, et al. An
618 improved genome release (version mt4. 0) for the model legume *Medicago truncatula*.
619 *BMC genomics*, 15(1):1, 2014.

620 Benjamin Vernot and Joshua M. Akey. Resurrecting surviving neandertal lineages from
621 modern human genomes. *Science*, 2014. doi: 10.1126/science.1245938. URL <http://www.sciencemag.org/content/early/2014/01/28/science.1245938.abstract>.

623 Ian J. Wang and Gideon S. Bradburd. Isolation by environment. *Molecular Ecology*, 23
624 (23):5649–5662, 2014. ISSN 1365-294X. doi: 10.1111/mec.12938. URL [http://dx.doi.](http://dx.doi.org/10.1111/mec.12938)
625 [org/10.1111/mec.12938](http://dx.doi.org/10.1111/mec.12938).

626 Andreas Weingessel and Kurt Hornik. Local PCA algorithms. *Neural Networks, IEEE*
627 *Transactions on*, 11(6):1242–1250, 2000.

628 Sewall Wright. The genetical structure of populations. *Annals of Eugenics*, 15(1):323–354,
629 1949. ISSN 2050-1439. doi: 10.1111/j.1469-1809.1949.tb02451.x. URL [http://dx.doi.](http://dx.doi.org/10.1111/j.1469-1809.1949.tb02451.x)
630 [org/10.1111/j.1469-1809.1949.tb02451.x](http://dx.doi.org/10.1111/j.1469-1809.1949.tb02451.x).

631 Jian Yang, Noah A Zaitlen, Michael E Goddard, Peter M Visscher, and Alkes L Price.
632 Advantages and pitfalls in the application of mixed-model association methods. *Nat*

635 A Choosing window length

636 The choice of window length entails a balance between signal and noise. In very short
637 windows, genealogies of the samples will only be represented by a few trees, so varia-
638 tion between windows represents demographic noise rather than meaningful variation in
639 patterns of relatedness. Longer windows generally have more distinct trees (and SNPs), al-
640 lowing for less noisy estimation of local patterns of relatedness. However, to better resolve
641 meaningful signal, i.e., differences in patterns of relatedness along the genome, we would
642 like reasonably short windows.

643 Since we summarize patterns of relatedness using relative positions in the principal
644 component maps, we quantify “noise” as the standard error of a sample’s position on PC1
645 in a particular window, averaged across windows and samples, and “signal” as the standard
646 deviation of the sample’s position on PC1 over all windows, averaged over samples. (Recall
647 that the signs for PCs are chosen to match each other.) Then, the mean variance across
648 windows is

$$\sigma_{\text{signal}}^2 = \frac{1}{N} \sum_{j=1}^N \frac{1}{L} \sum_{i=1}^L (PC1_{ij} - \overline{PC1}_j)^2,$$

649 where $PC1_{ij}$ is the position of the i^{th} individual on PC1 in window j , and $\overline{PC1}_j =$
650 $(1/N) \sum_{i=1}^N PC1_{ij}$. We estimate the standard error for each $PC1_{ij}$ using the block jack-
651 knife (Busing et al. 1999; Efron 1982): we divide the j^{th} window into 10 equal-sized
652 pieces, and let $PC1_{ij,k}$ denote the first principal component of this region found af-
653 ter removing the k^{th} piece; then the estimate of the squared standard error is $\sigma_{ij}^2 =$
654 $\frac{9}{10} \sum_{k=1}^{10} (PC1_{ij,k} - \frac{1}{10} \sum_{\ell=1}^{10} PC1_{ij,\ell})^2$. Averaging over samples and windows,

$$\sigma_{\text{noise}}^2 = \frac{1}{N} \sum_{j=1}^N \frac{1}{L} \sum_{i=1}^L \sigma_{ij}^2.$$

655 For the main analysis, we defined windows to each consist of the same number of neigh-
656 boring SNPs, and calculated σ_{signal}^2 and σ_{noise}^2 for a range of window sizes (i.e., numbers
657 of SNPs). For our main results we chose the smallest window for which σ_{signal}^2 was con-
658 sistently larger than σ_{noise}^2 (but checked other sizes); the values for various window sizes
659 across *Drosophila* chromosomes are shown in Table S1. In the cases we examined, we found
660 nearly identical results after varying window size, and choosing windows to be of the same
661 physical length (in bp) rather than in numbers of SNPs.

chrom. arm		window length (SNPs)				
		100	500	1,000	10,000	100,000
2L	σ_{noise}^2	2.05	1.64	1.18	0.17	0.04
	σ_{signal}^2	2.76	2.69	2.23	0.68	0.31
2R	σ_{noise}^2	2.18	1.92	1.63	0.58	0.13
	σ_{signal}^2	2.78	2.70	2.65	2.31	1.82
3L	σ_{noise}^2	2.08	2.00	1.64	0.73	0.25
	σ_{signal}^2	2.60	2.52	2.40	1.68	1.89
3R	σ_{noise}^2	1.95	1.76	1.44	0.59	0.20
	σ_{signal}^2	2.58	2.51	2.44	1.96	1.40
X	σ_{noise}^2	2.48	2.04	1.54	1.62	0.17
	σ_{signal}^2	2.61	2.43	2.30	0.32	1.14

Table S1: Measures of signal and noise, computed separately for each chromosome arm in the *Drosophila* dataset, at different window sizes. All values are multiplied by 1,000 (so typical variation is of order of 50% of the actual values). Starting at windows of 1,000 SNPs, the signal (variation of PC1 between windows) starts to be substantially larger than the noise (standard error of PC1 for each window).

B Weighted PCA

Principal components analysis can be thought of as finding a good low-dimensional matrix factorization (Engelhardt and Stephens 2010) that well-approximates the original data in the least-squares sense: if C is the $N \times N$ genetic covariance matrix, then to find the top k principal components, we find an orthogonal $N \times k$ matrix U , and a $k \times k$ diagonal matrix Λ with diagonal entries $\Lambda_{ii} = \lambda_i$ to minimize

$$\|C - U\Lambda U^T\|^2 = \sum_{ij} \left(C_{ij} - \sum_m \lambda_m U_{im} U_{jm} \right)^2. \quad (3)$$

The columns of U , known as the principal components, are the eigenvectors of C , the entries of λ are the eigenvalues of C , and the proportion of variance explained by the m^{th} component is

$$\frac{\lambda_m^2}{\sum_{\ell} \lambda_{\ell}^2} = \frac{\sum_{ij} (\lambda_m U_{im} U_{jm})^2}{\sum_{ij} C_{ij}^2}.$$

Thinking about the problem as a least-squares approximation problem makes it clear why unbalanced sample sizes can result in undesirable outcomes. If we want to describe variation *between* populations, but 80% of the samples are from a single population, then unless populations are highly differentiated, a better approximation to C may be obtained

by using the columns of U to describe variation *within* the overrepresented population rather than between the populations. A common workaround is to remove samples, but a more elegant solution can be found by reweighting the objective function in (3). Let w_i be a weight associated with sample i , W the diagonal matrix with w along the diagonal, and instead seek to minimize

$$\|W^{1/2}(C - U\Lambda U^T)W^{1/2}\|^2 = \sum_{ij} w_i w_j \left(G_{ij} - \sum_m \lambda_m U_{im} U_{jm} \right)^2, \quad (4)$$

and now for convenience we require U to be orthogonal in $\ell_2(w)$, i.e., that $U^T W U = I$. We then would choose w to give roughly equal weight to each *population*, instead of each individual. We have used with good results the weightings $w_i = 1/\max(10, n_i)$, where n_i is, if there are discrete populations, the number of samples in the same population as sample i ; or, for continuously sampled individuals, the number of samples within a certain distance of sample i .

To solve (4), let λ and V denote the top k eigenvalues and eigenvectors of $W^{1/2} C W^{1/2}$, so that $V \Lambda V^T$ is the rank k matrix closest in least squares to $W^{1/2} C W^{1/2}$; so if we define $U = W^{-1/2} V$ then $U^T W U = V^T V = I$, and

$$W^{-1/2} V \Lambda V^T W^{-1/2} = U \Lambda U^T$$

is the low-dimensional approximation to C . The proportion of variance explained is calculated from eigenvalues as before, but has the interpretation

$$\frac{\lambda_m^2}{\sum_{\ell} \lambda_{\ell}^2} = \frac{\sum_{ij} w_i w_j (\lambda_m U_{im} U_{jm})^2}{\sum_{ij} w_i w_j C_{ij}^2}.$$

In our R implementation we use the Spectra library (Qiu and Mei 2016) to find only the top k eigenvectors.

C Supplementary Tables

	10000snp, 2 PCs	1000snp, 2 PCs	10000snp, 5 PCs	100000bp, 2 PCs	10000bp, 2 PCs
10000snp, 2 PCs	1.00	0.87	0.96	0.90	0.90
1000snp, 2 PCs	0.68	1.00	0.73	0.68	0.68
10000snp, 5 PCs	0.96	0.92	1.00	0.88	0.88
100000bp, 2 PCs	0.90	0.87	0.88	1.00	1.00
10000bp, 2 PCs	0.68	0.93	0.72	0.67	0.67

[[2]]

	MDS1	10000 SNPs, 2 PCs	1000 SNPs, 2 PCs	10000 SNPs, 5 PCs	100000bp, 2 PCs	100000bp, 5 PCs
10000 SNPs, 2 PCs		1.00	0.54	0.93	0.87	0.83
1000 SNPs, 2 PCs		0.82	1.00	0.76	0.83	0.83
10000 SNPs, 5 PCs		0.93	0.50	1.00	0.84	1.00
100000bp, 2 PCs		0.87	0.59	0.84	1.00	0.84
100000bp, 5 PCs		0.83	0.92	0.77	0.84	1.00
	MDS2	10000snp, 2 PCs	1000snp, 2 PCs	10000snp, 5 PCs	100000bp, 2 PCs	100000bp, 5 PCs
10000snp, 2 PCs		1.00	0.54	0.93	0.87	0.83
1000snp, 2 PCs		0.82	1.00	0.76	0.83	0.83
10000snp, 5 PCs		0.93	0.50	1.00	0.84	1.00
100000bp, 2 PCs		0.87	0.59	0.84	1.00	0.84
100000bp, 5 PCs		0.83	0.92	0.77	0.84	1.00

Table S2: C

correlations between MDS coordinates of genomic regions between runs with different parameter values. To produce these, we first ran the algorithm with the specified window size and number of PCs (k in equation [XXX](#)) on the full *Medicago truncatula* dataset. Then to obtain the correlation between results obtained from parameters A in the row of the matrix above and parameters B in the column of the matrix above, we mapped the windows of B to those of A by averaging MDS coordinates of any windows of B whose midpoints lay in the corresponding window of A; we then computed the correlation between the MDS coordinates of A and the averaged MDS coordinates of B. This is not a symmetric operation, so these matrices are not symmetric. As expected, parameter values with smaller windows produce noisier estimates. Plots of MDS values along the genome are visually nearly identical for parameter sets having similar window sizes – full reports are available as supplementary material on Data Dryad [XXX](#).

695 D Supplementary Figures

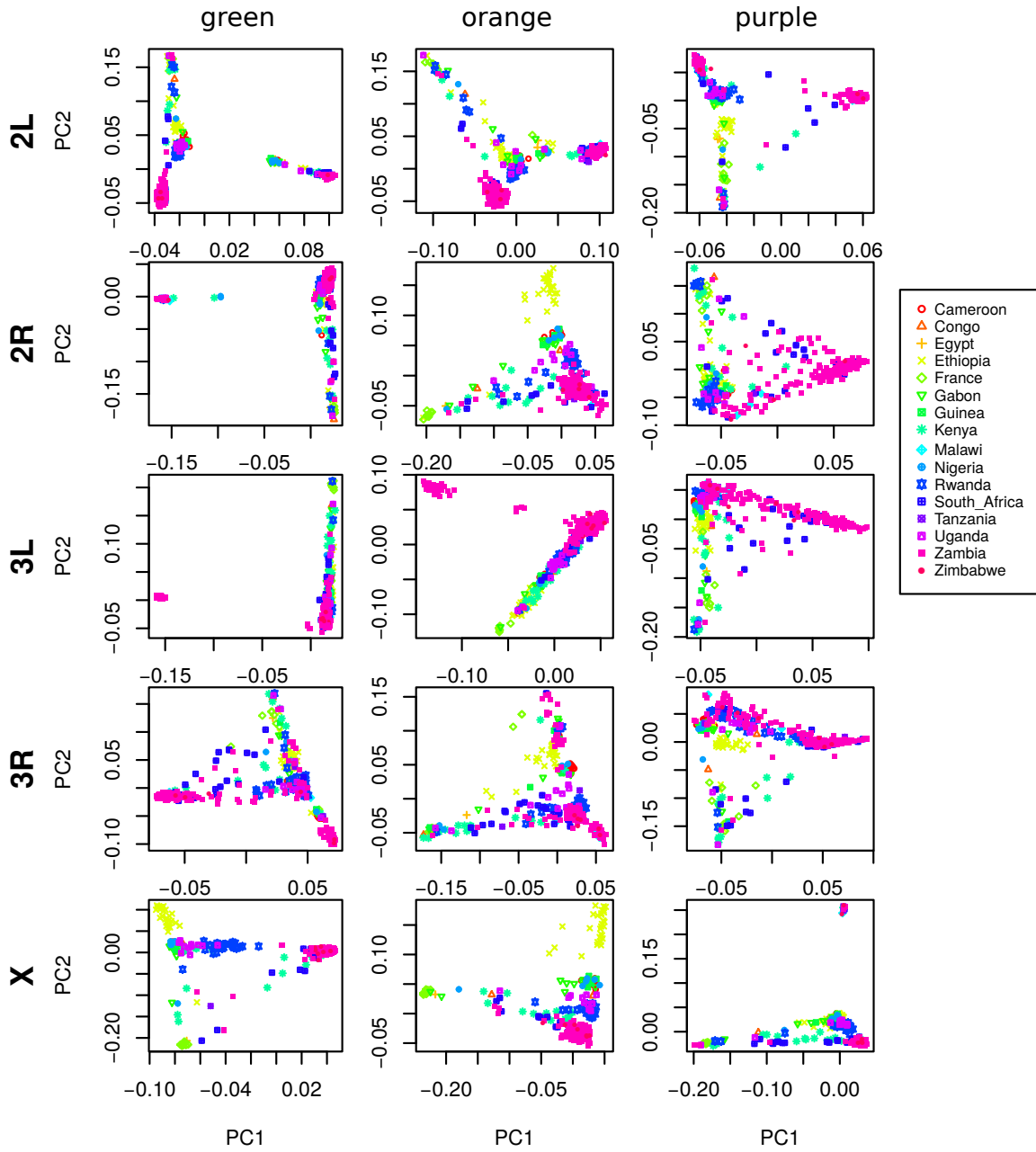


Figure S1: PCA plots for the three sets of genomic windows colored in Figure 2, on each chromosome arm of *Drosophila melanogaster*. In all plots, each point represents a sample. The first column shows the combined PCA plot for windows whose points are colored green in Figure 2; the second is for orange windows; and third is for purple windows.

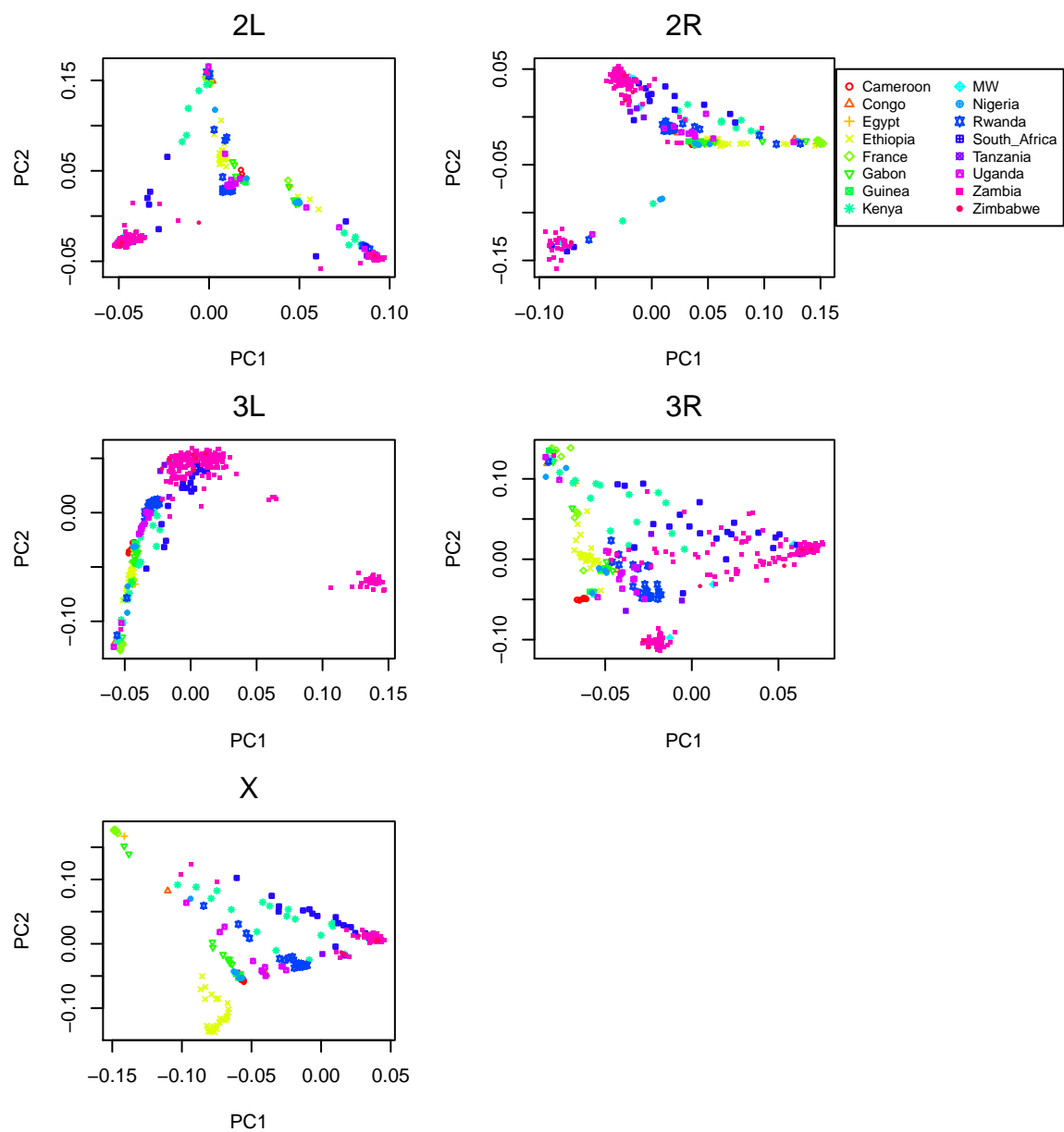


Figure S2: PCA plots for chromosome arms 2L, 2R, 3L, 3R and X of the *Drosophila melanogaster* dataset.

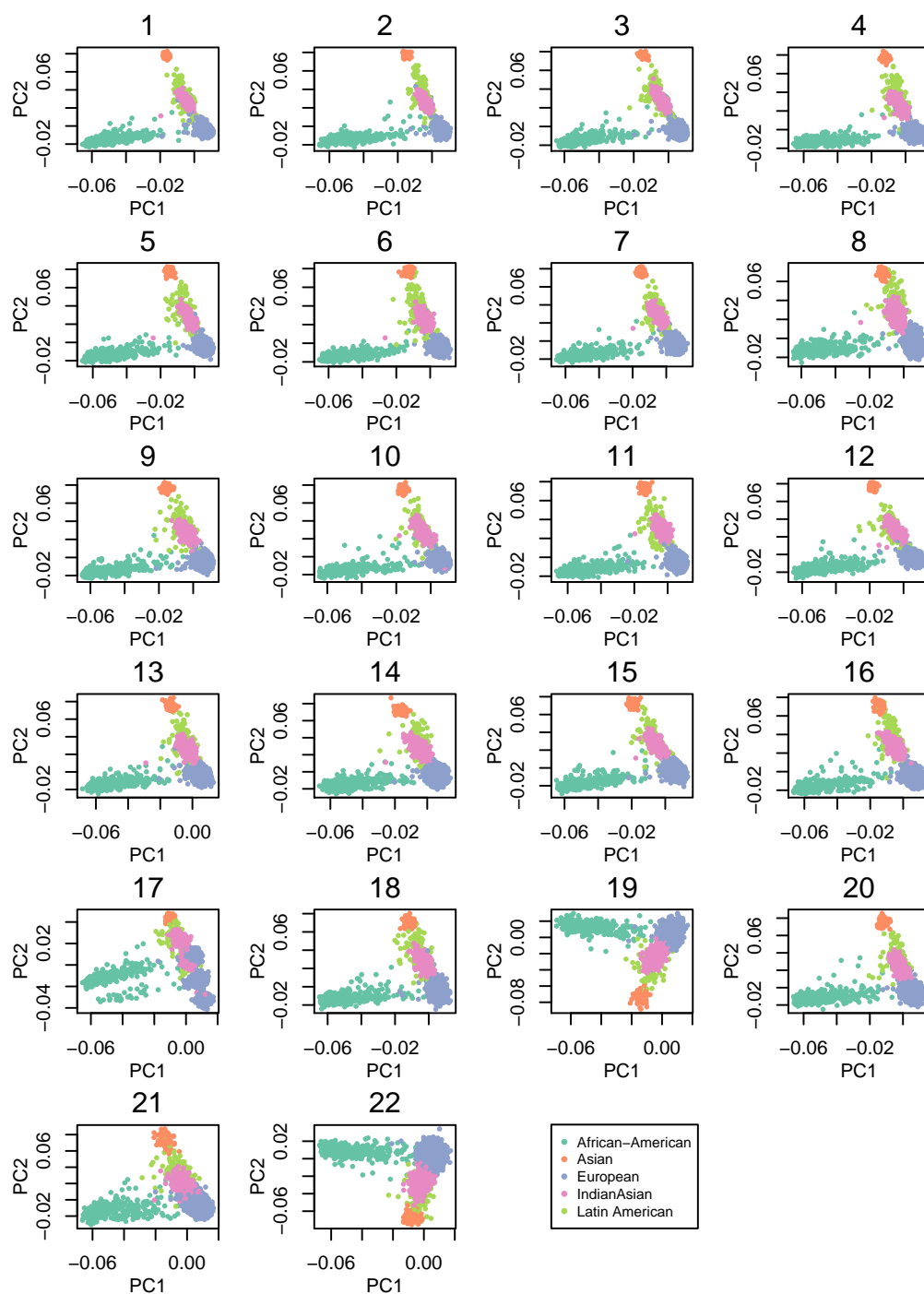


Figure S3: PCA plots for all 22 human autosomes from the POPRES data.

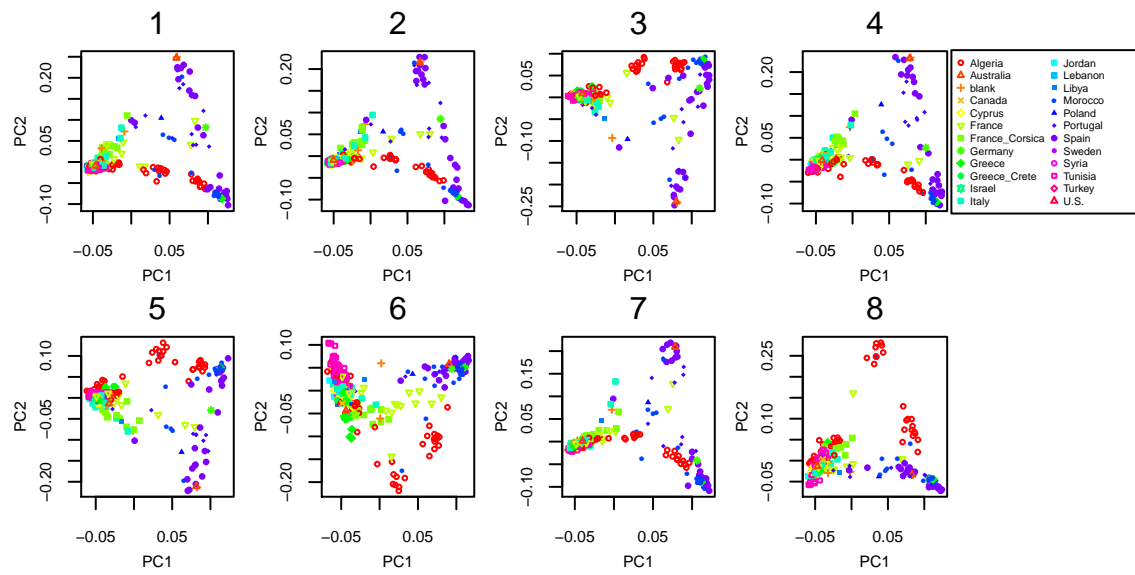


Figure S4: PCA plots for all 8 chromosomes in the *Medicago truncatula* dataset.

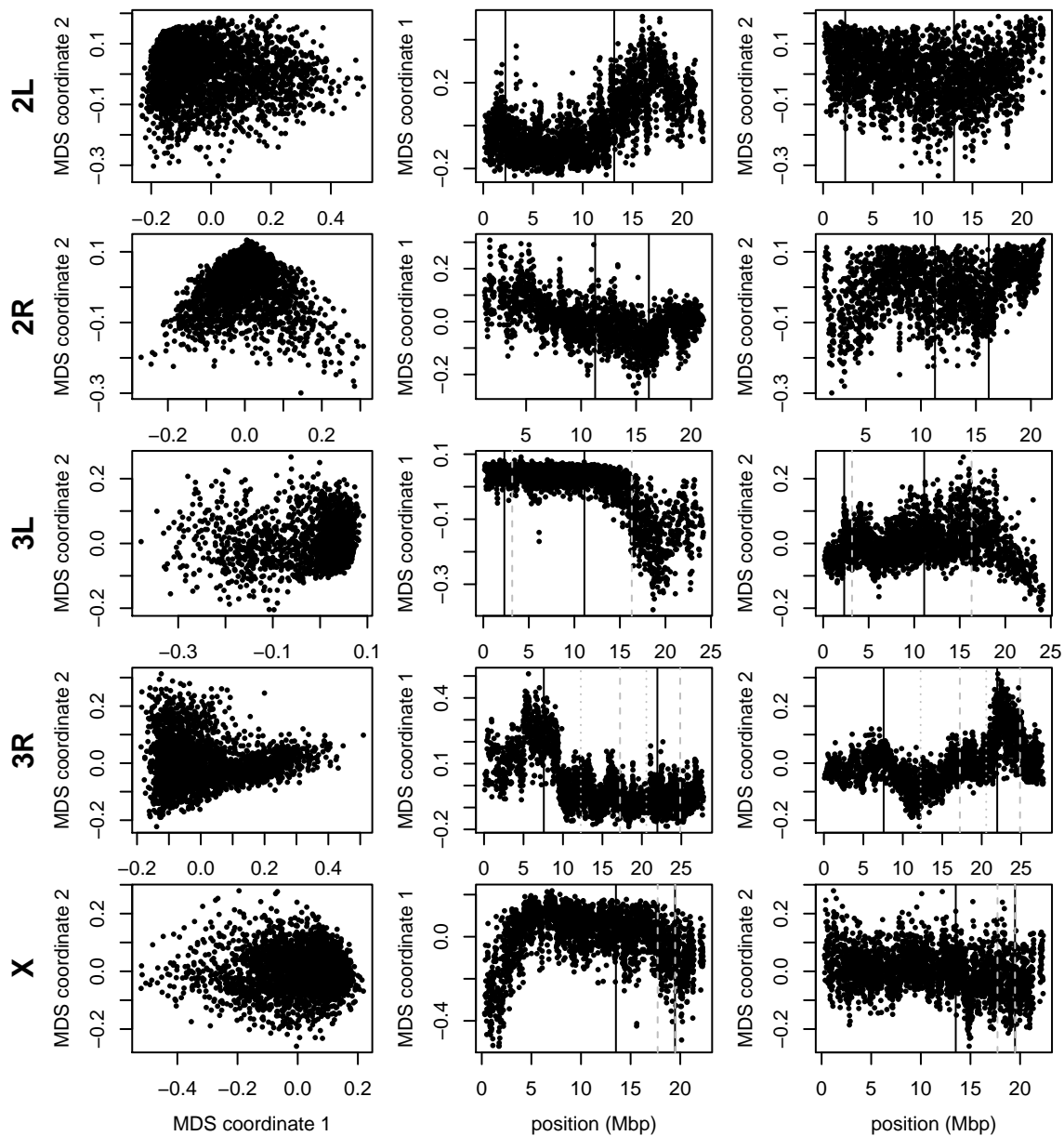


Figure S5: Variation in structure for windows of 1,000 SNPs across *Drosophila melanogaster* chromosome arms: without inversions. As in Figure 2, but after omitting for each chromosome arm individuals carrying the less frequent orientation of any inversions on that chromosome arm. The values differ from those in 4 in the window size used and that some MDS values were inverted (but relative orientation is meaningless as chromosome arms were run separately, unlike for *Medicago*). In all plots, each point represents one window along the genome. The first column shows the MDS visualization of relationships between windows, and the second and third columns show the midpoint of each window against the two MDS coordinates; rows correspond to chromosome arms. Colors are consistent for plots in each row. Vertical lines show the breakpoints of known polymorphic inversions.

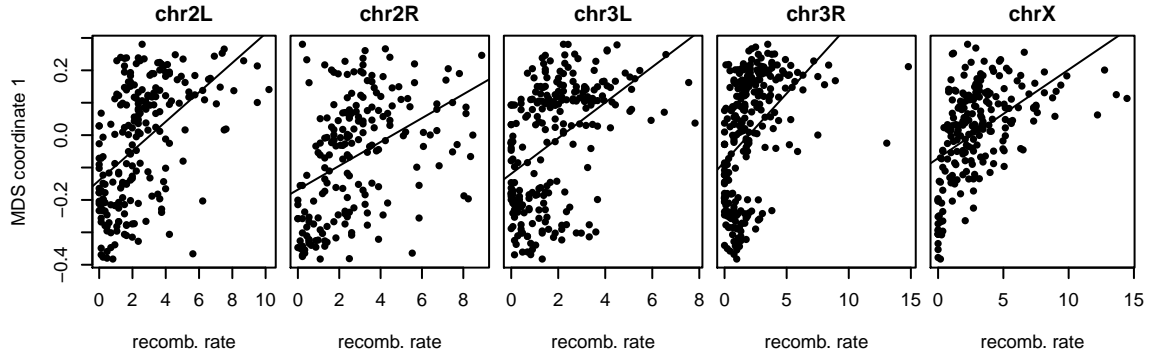


Figure S6: Recombination rate, and the effects of population structure for *Drosophila melanogaster*: this shows the first MDS coordinate and recombination rate (in cM/Mbp), as in Figure 4, against each other. Since the windows underlying estimates of Figure 4 do not coincide, to obtain correlations we divided the genome into 100Kbp bins, and for each variable (recombination rate and MDS coordinate 1) averaged the values of each overlapping bin with weight proportional to the proportion of overlap. The correlation coefficient and p -values for each linear regression are as follows: 2L: correlation = 0.52, $r^2 = 0.27$; 2R: correlation = 0.43, $r^2 = 0.18$; 3L: correlation = 0.47, $r^2 = 0.21$; 3R: correlation = 0.46, $r^2 = 0.21$; X: correlation = 0.50, $r^2 = 0.24$.

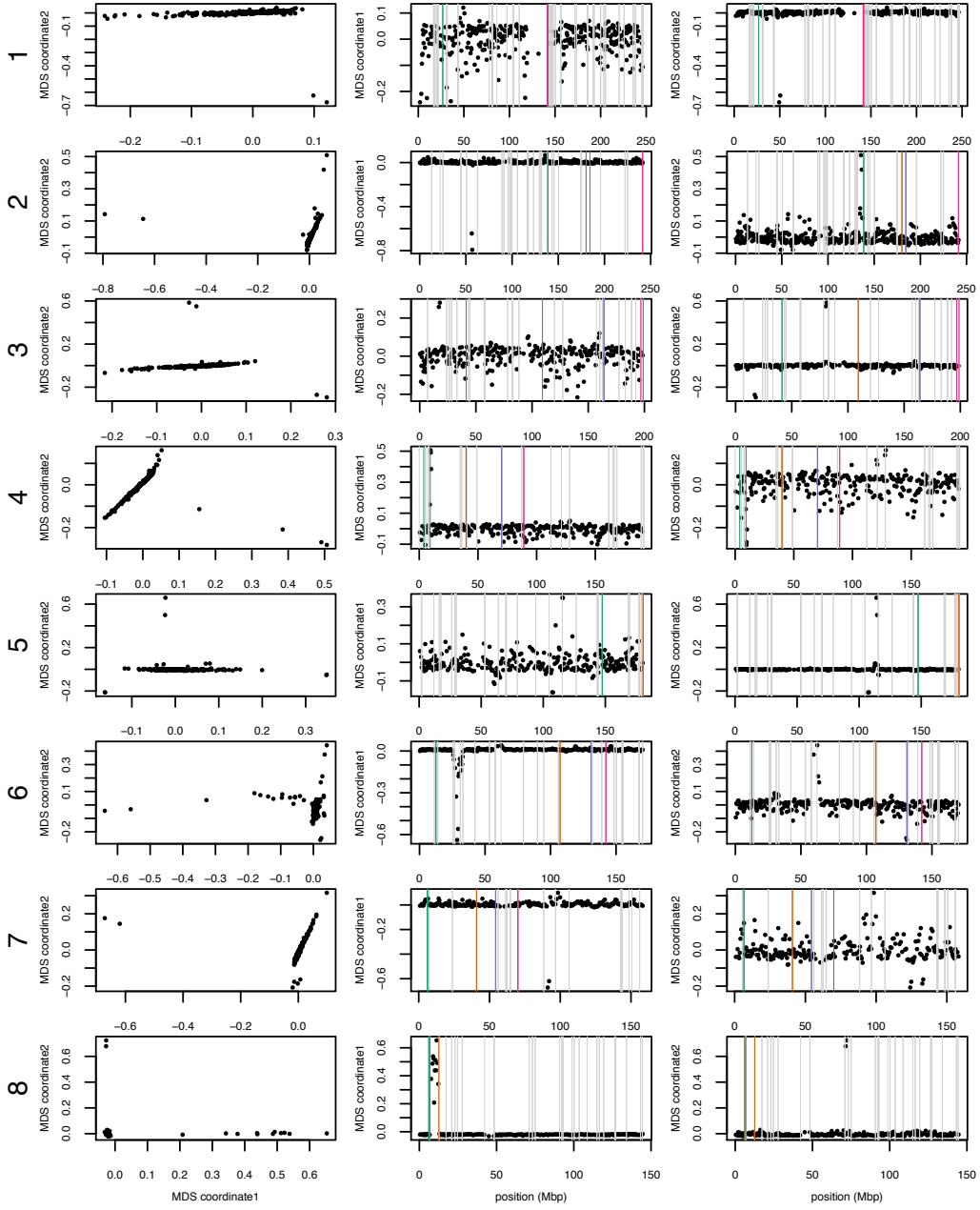


Figure S7: MDS plots for human chromosomes 1-8. The first column shows the MDS visualization of relationships between windows, and the second and third columns show the midpoint of each window against the two MDS coordinates; rows correspond to chromosomes. Colorful vertical lines show the breakpoints of known valid inversions, while grey vertical lines show the breakpoints of predicted inversions.

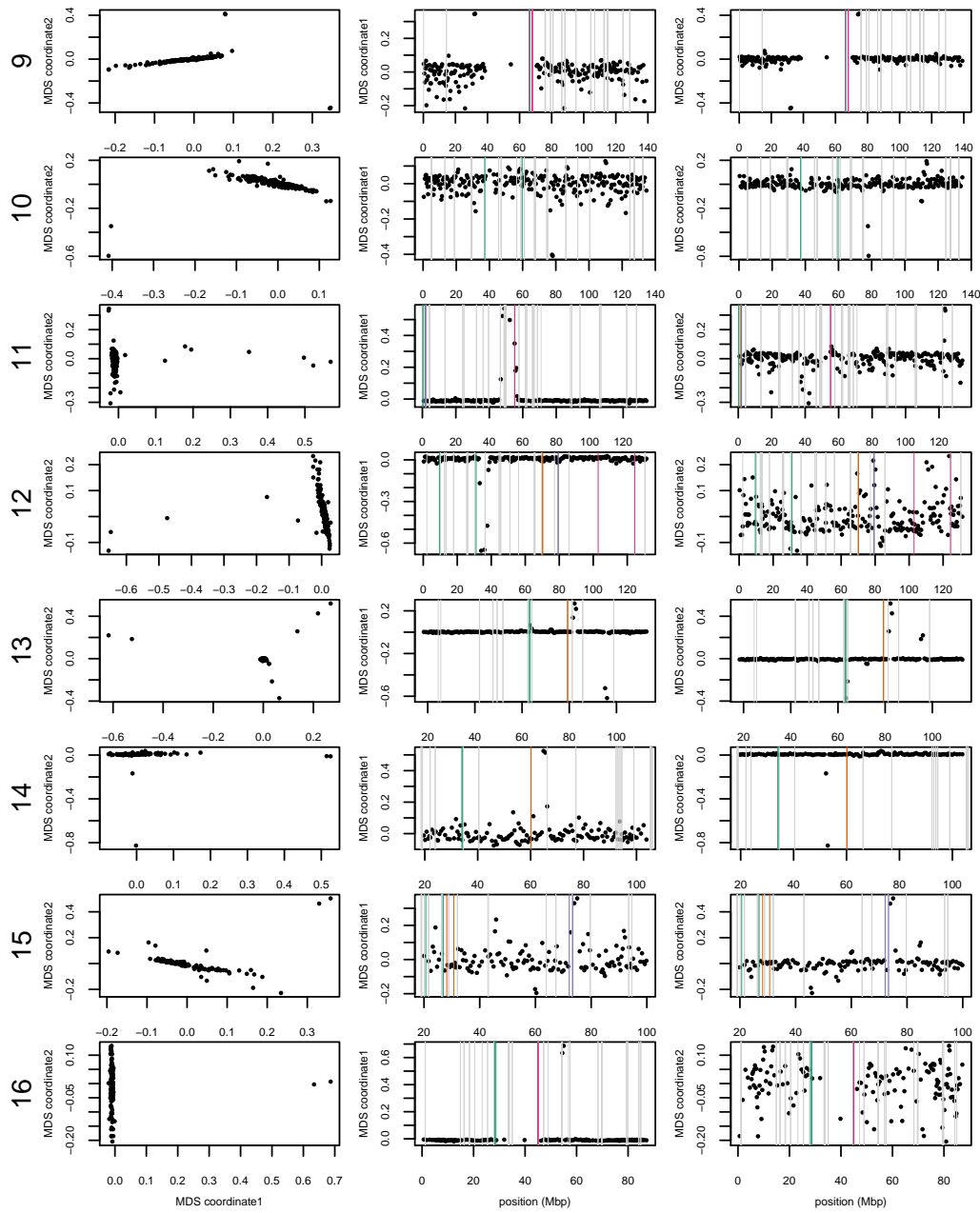


Figure S8: MDS plots for human chromosomes 9-16, as in Supplemental Figure S7.

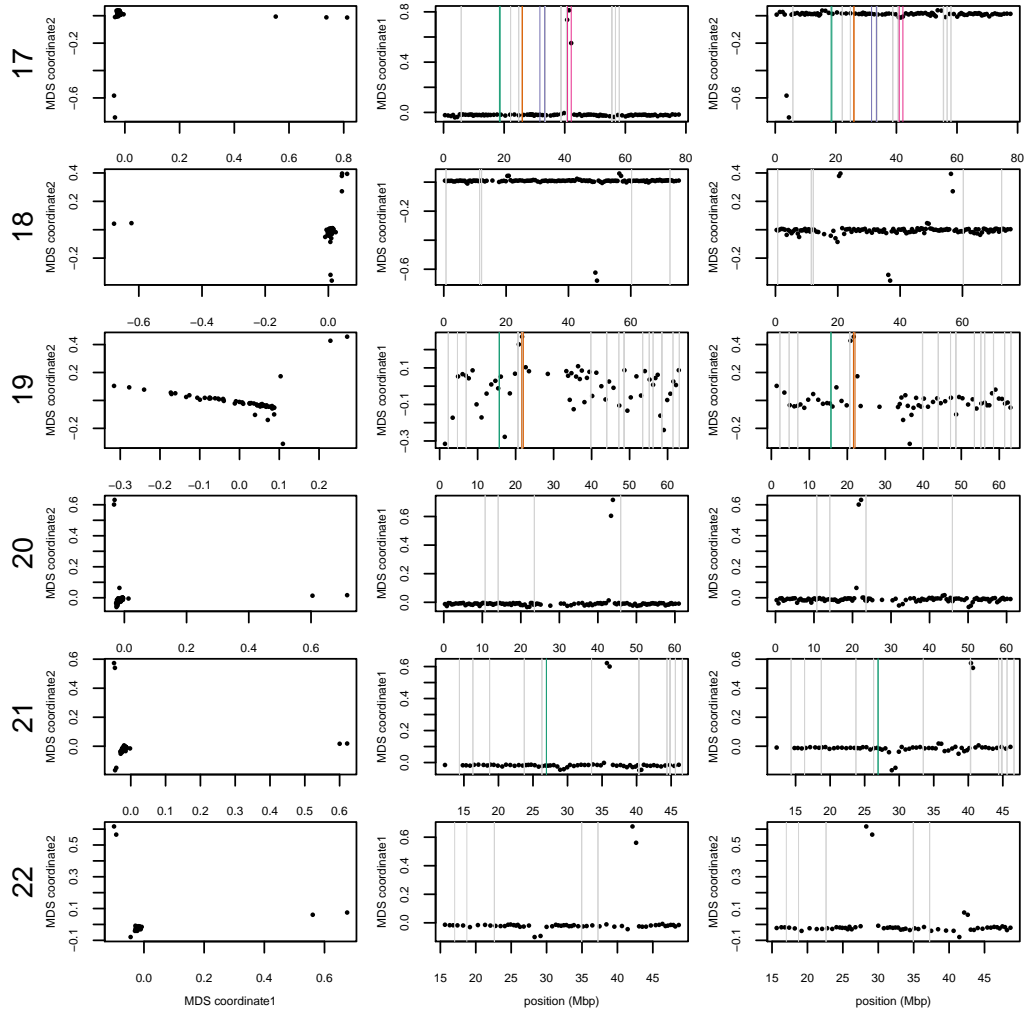


Figure S9: MDS plots for human chromosomes 17-22, as in Supplemental Figure S7.

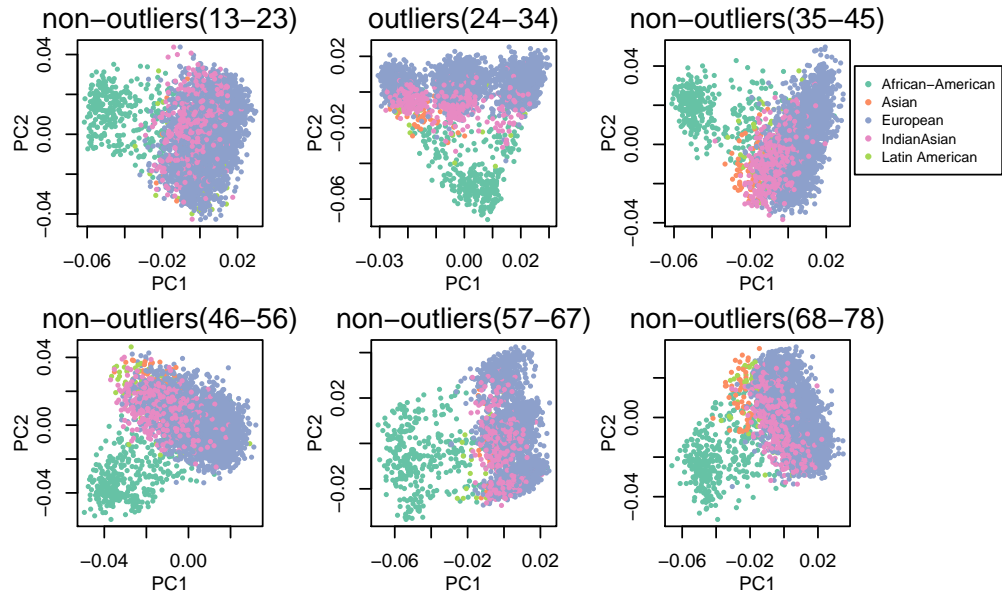


Figure S10: Comparison of PCA figures within outlying windows (center column) and flanking non-outlying windows (left and right columns) for the two windows having outlying MDS scores on chromosome 8.

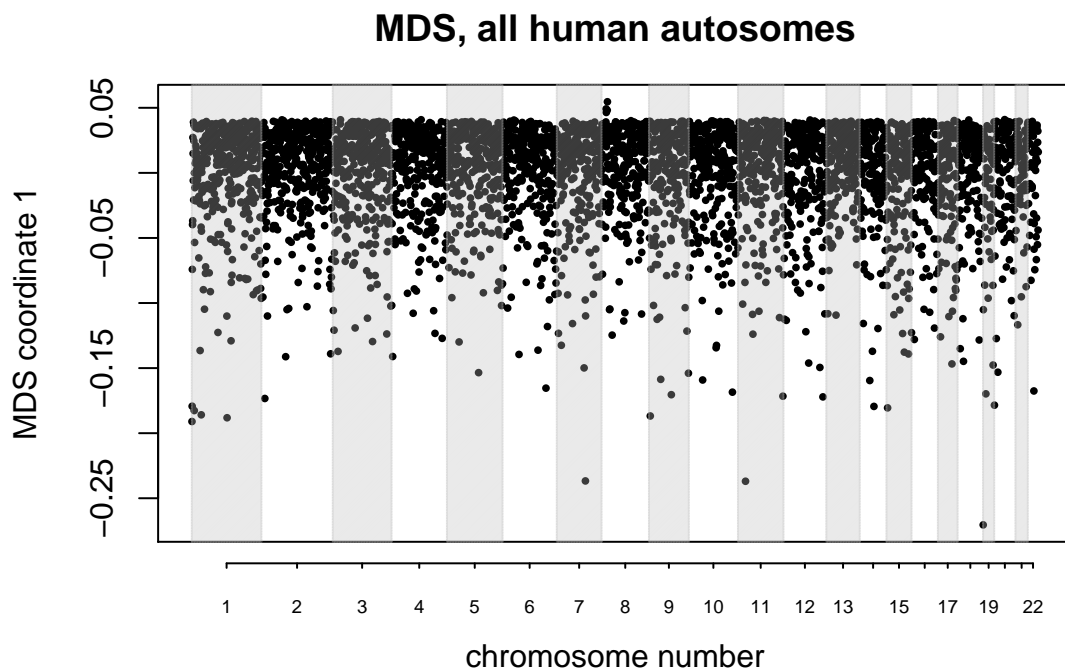


Figure S11: MDS visualization of variation in the effects of population structure amongst windows across *all* human autosomes simultaneously. The small group of windows with positive outlying MDS values lie around the inversion at 8p23.

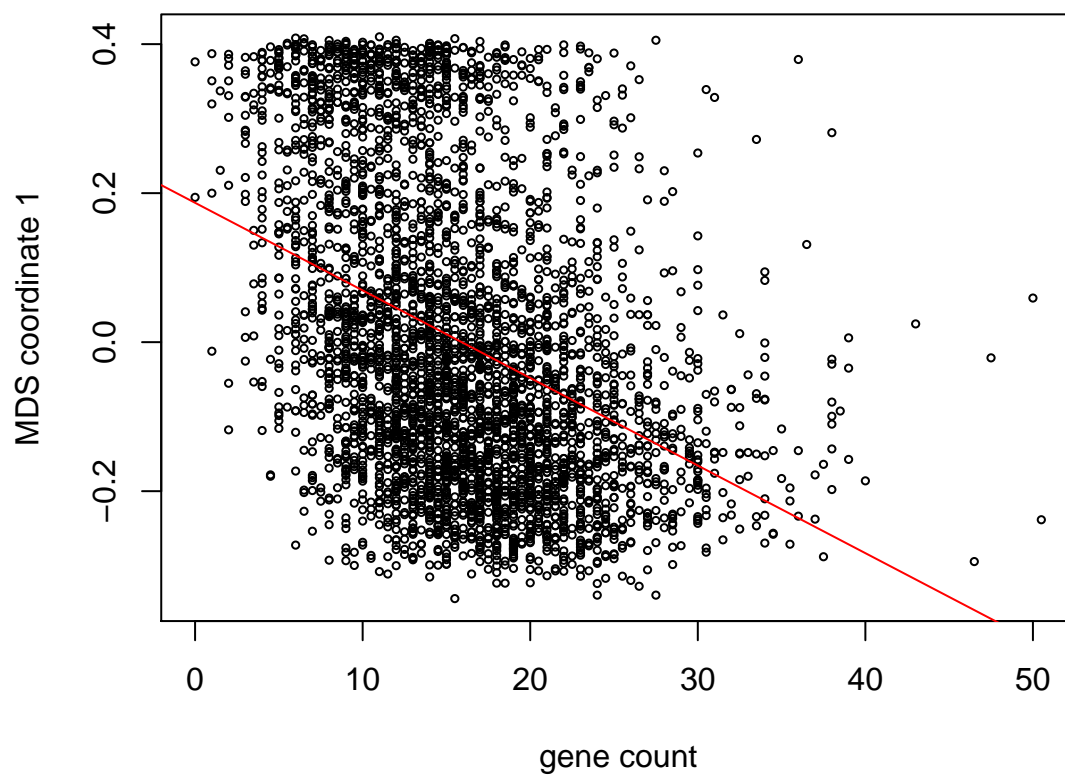


Figure S12: First MDS coordinate against gene density for all 8 chromosomes of *M. truncatula*. The first MDS coordinate is significantly correlated with gene count ($r = 0.149$, $p = 2.2 \times 10^{-16}$).

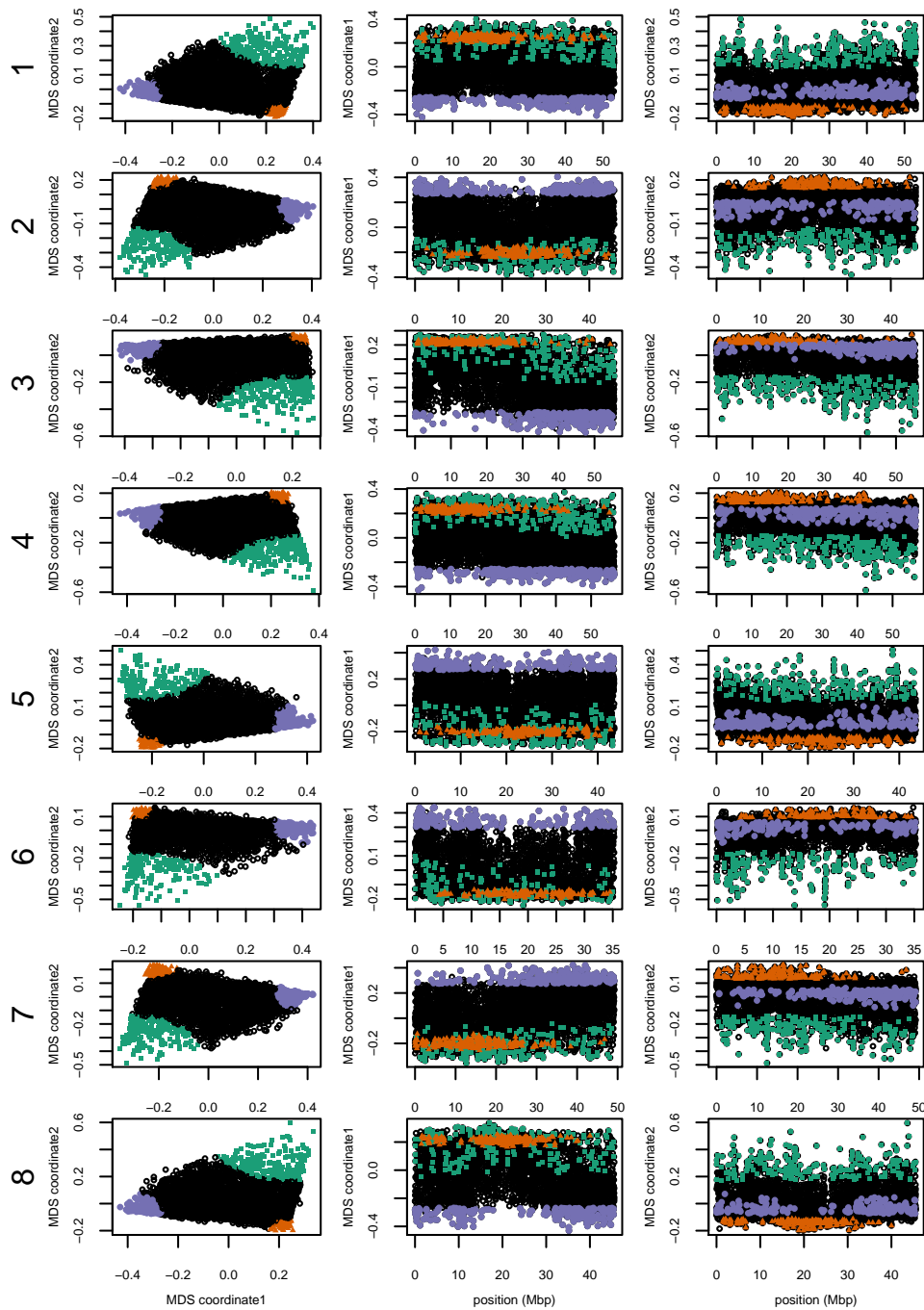


Figure S13: MDS visualizations of the effects of population structure for all 8 chromosomes of the *Medicago truncatula* data.

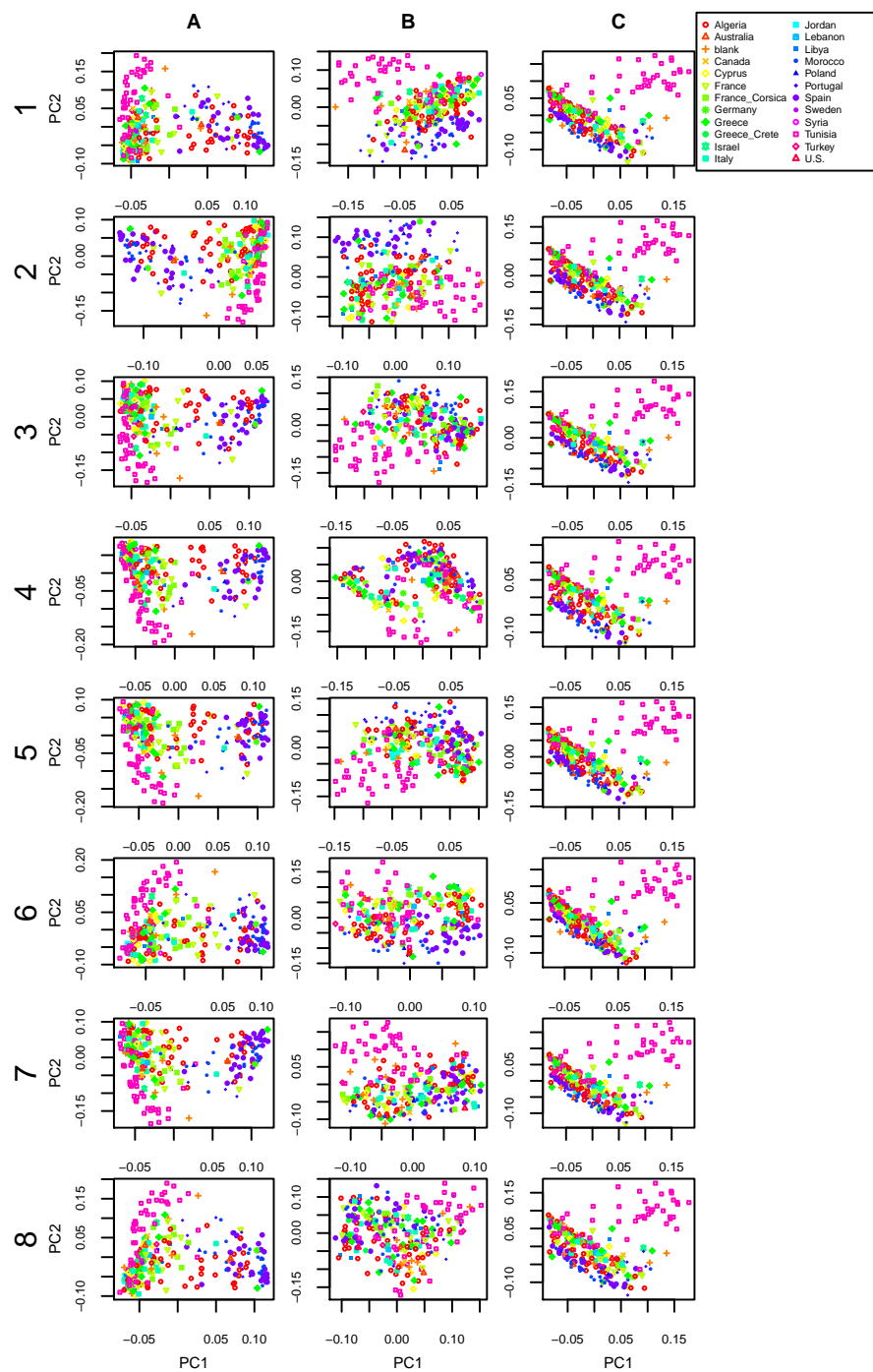


Figure S14: PCA plots for regions colored in Figure S13 on all 8 chromosomes of *Medicago truncatula*: (A) green, (B) orange, and (C) purple.

Resubmission Cover Letter
Genetics

Han Li
and Peter Ralph
June 14, 2017

To the Editor(s) –

We are pleased to submit a revision of our manuscript,
Sincerely,

Han Li and Peter Ralph

Reviewer AE:

Please understand that incremental changes will not be sufficient. Adding simulations to strengthen key claims will be necessary, particularly addressing the impacts of mutation rate and recombination rate variation with more depth, the concern regarding PC switching (Reviewer 1), and the concern regarding the impacts of variation in missingness by sub-population (Reviewer 2).

Reviewer 1:

The paper is generally well written and clear; it addresses an important problem, and clearly makes some progress on it. However, it suffers from having no grounding in either theory or empirical demonstration that it really can find the structures that are claimed. I find the arguments that it finds inversions compelling, though not watertight, and I am not yet convinced that it is finding ubiquitous background selection. To make this claim, significant extra work is required.

In short, the approach is interesting but not sufficiently explored to produce compelling evidence for the implications that are claimed. Putting a large amount of effort into simulations may alleviate these concerns somewhat.

Specific points: What does this method find? I'm concerned about: (a) variation in the recombination rate and (b) variation in the mutation rate, creating spurious structure.

The first possibility is that massively varying information quantity within windows could lead to a small number of such windows having their orientation reversed: that is, PC1 becomes PC2 and vice versa. (Or PC2 and PC3 could switch). This would lead to such windows having unusual properties and hence appearing as evidence of an inversion.

I do agree with the authors that significant outliers would be found at inversions. However, even if the PC switching does not occur, or the model could handle it, the evidence for selection is weaker. If the two types of variation described above exist, with no selection, I would still expect a "continuous triangle" of results (as seen left of Fig 2, top left of Fig 6) with extrema described by windows with the most information, and points placed at different extremum having low recombination rate (because by chance, these will get an approximately fixed local tree, corresponding on average to the genome-wide population structure).

Addressing this is likely quite hard, though the authors may be able to think of something that separates these effects from selection.

(1.1) ... variation in the recombination rate ...

(1.2) ... and variation in the mutation rate, creating spurious structure.

(1.3) **PC switching** ... could lead to a small number of such windows having their orientation reversed: that is, PC1 becomes PC2 and vice versa. (Or PC2 and PC3 could switch).

(1.4) **p6** “here, we use $k=2$...” - you have to show that $k > 2$ is the same.

(1.5) **p15** “We also found nearly identical results when choosing shorter windows of 1,000 SNPs” - again, show this.

(1.6) **p15** “or choosing windows of equal length in base pairs rather than SNPs” - once again.

(1.7) Using 2 PCs is common practice: only if this is the end of an analysis and the PCA was done for visualisation. Here you are using it for something so should keep all the relevant PCs.

(1.8) I’m surprised that PCAdmix isn’t referenced. It is using a very similar method, albeit with different goals. In particular, the approach of placing all points into a single, genome-wide PC space solves many of the problems that this approach has (though I agree there may be benefits to the approach described here)

Reviewer 2:

This is an interesting and well written paper. It was a pleasant read. I have three main general comments:

(2.1) **Related work:** The authors provide an introduction of the main concepts, as well as some intuition of what the method is doing and how, but I found comparison to previous approaches to be somewhat missing. To some extent, this is due to the fact that the main goal of their analysis is somewhat vaguely “finding heterogeneity”, which leads to the applications of detecting chromosomal inversions and evidence for background selection. It would help to have a well defined set of hypotheses, test the method’s accuracy using simulation (see next comment), and compare to previous efforts in similar domains.

(2.2) Validation: In several occasions, the authors seem to introduce a potential problem in their approach, and provide a solution to it. This is generally rather intuitive, but it would really help to have simulations of some sort to show that the issue arises and leads to a problem, and that their approach does address the specific problem.

(2.3) The use of weighted PCA to cope with unbalanced sample size could be better demonstrated. Although the current explanation makes intuitive sense, this approach does not seem to be used in previous work. The authors could design a simulation that supports their approach.

(2.4) It is conceivable that some subpopulations will have more missingness in some windows. That may skew the resulting PCs by selecting different sample sizes for the different windows (as discussed in Appendix B). This could distort the PCs, so that variation reflects underlying variation in missingness. Would be good to discuss this potential issue and provide simulations.

(2.5) Appendix A: when using jackknife to estimate variance, each window is being divided in 10 “independent” resampling units. Due to LD, these 10 blocks are likely correlated, which would bias the estimates of variance. This is probably not a problem because both signal and noise could be equally biased, but the authors may want to consider this potential issue. I wonder if the correlation with recombination rate may be partially explained by this.

(2.6) Is it possible to explain the results of Figure 6 just considering neutral variation in local ancestry due to recent admixture? This may explain why ancestry seems to explain a fair amount of variance in the lower plots of Fig 6. Local PCA has been previously used by others to detect local ancestry blocks, e.g. see the PCAdmix approach by Brisbin et al. The authors discuss the possibility that admixture is driving the differentiation, but do not test whether their observations agree with neutrality.

(2.7) “to remove the effect of artifacts such as mutation rate variation, we also rescale each approximate covariance matrix to be of similar size (precisely, so that the underlying data matrix has trace norm equal to one”. This potential issue is a bit unclear to me, since I would expect that scaling the volume of local trees would not result in changed distances in PC space. Perhaps the authors could show via simulations that this creates a problem, and that the normalization addresses it.

(2.8) Figure 7: are MDS coordinates correlated with recombination rates in this case?

(2.9) Application: *is what the authors seem to be proposing not already accounted for by linear mixed model association approaches? If not, this should be clarified. Either way, this paragraph could be dropped.*

(2.10) Introduction: *“it is not necessarily clear what aspects of demography should be included in the concept.” I find it a bit weird to describe selection as an “aspect of demography”. Although it could be seen as such within a coalescent framework, that seems to be just a useful representation. The authors may consider rewording’.*

(2.11) *Paragraph starting in “Since the definition...”. The notation is a bit unclear. Please check that it is clear which PC the text refers to.*

(2.12) *Would the authors be able to provide a sense for the directionality of effects in Figure 4? It would be interesting if the authors tried to further characterize regions that are similar due to higher recombination rates. E.g. is there more/less density of polymorphisms in these regions?*

(2.13) Page 13: *typo: “figures 6 and 6”.*

(2.14) *Typo in abstract, line 6 “, We show” -> “. We show”.*

(2.15) *Typo: end of introduction “an visualization”. The whole sentence is a bit weird. The authors just stated focus is on clustering, not on looking for outliers, but what does it mean that “we allow ourselves to be surprised by unexpected signals in the data”?*

(2.16) *“There has been substantial debate over the relative impacts of different forms of selection.” Citation needed.*

(2.17) *“Results using larger numbers of PCs were nearly identical”. It would be interesting to have a supplementary table.*

(2.18) *Table 1 legend seems a bit redundant. Columns are self-explanatory.*

(2.19) *It would help to have numbered lines and references.*
